

Review

# Enhancement of the Detection Performance of Paper-Based Analytical Devices by Nanomaterials

Renzhu Pang<sup>1</sup>, Qunyan Zhu<sup>2</sup>, Jia Wei<sup>1,2</sup>, Xianying Meng<sup>1,\*</sup> and Zhenxin Wang<sup>2,3,\*</sup> 

<sup>1</sup> Department of Thyroid Surgery, The First Hospital of Jilin University, Changchun 130021, China; pangrenzhu@jlu.edu.cn (R.P.); weijia@ciac.ac.cn (J.W.)

<sup>2</sup> State Key Laboratory of Electroanalytical Chemistry, Changchun Institute of Applied Chemistry, Chinese Academy of Sciences, Changchun 130022, China; zhuqy@ciac.ac.cn

<sup>3</sup> School of Applied Chemical Engineering, University of Science and Technology of China, Hefei 230026, China

\* Correspondence: mengxiany@mail.jlu.edu.cn (X.M.); wangzx@ciac.ac.cn (Z.W.)

**Abstract:** Paper-based analytical devices (PADs), including lateral flow assays (LFAs), dipstick assays and microfluidic PADs ( $\mu$ PADs), have a great impact on the healthcare realm and environmental monitoring. This is especially evident in developing countries because PADs-based point-of-care testing (POCT) enables to rapidly determine various (bio)chemical analytes in a miniaturized, cost-effective and user-friendly manner. Low sensitivity and poor specificity are the main bottlenecks associated with PADs, which limit the entry of PADs into the real-life applications. The application of nanomaterials in PADs is showing great improvement in their detection performance in terms of sensitivity, selectivity and accuracy since the nanomaterials have unique physicochemical properties. In this review, the research progress on the nanomaterial-based PADs is summarized by highlighting representative recent publications. We mainly focus on the detection principles, the sensing mechanisms of how they work and applications in disease diagnosis, environmental monitoring and food safety management. In addition, the limitations and challenges associated with the development of nanomaterial-based PADs are discussed, and further directions in this research field are proposed.

**Keywords:** paper-based analytical devices; nanomaterials; point-of-care testing; signal enhancement



**Citation:** Pang, R.; Zhu, Q.; Wei, J.; Meng, X.; Wang, Z. Enhancement of the Detection Performance of Paper-Based Analytical Devices by Nanomaterials. *Molecules* **2022**, *27*, 508. <https://doi.org/10.3390/molecules27020508>

Academic Editors: Giuseppe Cirillo, Chongjun Zhao and Sungsu Park

Received: 27 November 2021

Accepted: 10 January 2022

Published: 14 January 2022

**Publisher's Note:** MDPI stays neutral with regard to jurisdictional claims in published maps and institutional affiliations.



**Copyright:** © 2022 by the authors. Licensee MDPI, Basel, Switzerland. This article is an open access article distributed under the terms and conditions of the Creative Commons Attribution (CC BY) license (<https://creativecommons.org/licenses/by/4.0/>).

## 1. Introduction

As an easily accessible and cheap material made from cellulose (the most abundant polymer on earth) or nitrocellulose, paper offers many advantages for development of biosensing platforms, in particular point-of-care-testing (POCT) devices [1–7]. For instance, various in situ analyses can be achieved by the paper-based analytical devices (PADs) because many recognition probes, such as ligands, antibodies and aptamers, can be easily immobilized within the (nitro)cellulose matrix [8–20]. Because of the controlled porosity and capillary forces of the nitrocellulose/cellulose network, the fluidics can be efficiently transported via capillary flow. In addition, the PADs are compatible with different detection systems, including naked eye and simple optical or electrical readers, which meets the needs in developing countries [21–25]. In the past decades, PADs, including lateral flow assays (LFAs), dipstick assays and microfluidic PADs ( $\mu$ PADs), have been well developed and shown a great impact on the clinical diagnosis, environmental monitoring and food safety management [8–35]. For example, one type of PAD, the lateral flow immunoassay (LFIA), is commercially available and is extensively used as a powerful diagnostic platform for the rapid detection of antibodies or antigens at a low cost [34–36]. The LFIA has dominated the market of rapid diagnostic testing since the lateral flow immunochromatographic strip was first developed for screening the supernatants of hybridomas in 1982 through antigen–antibody interaction on paper to produce a color change visible to the naked eye [34–37].

The PADs detection methods include optical techniques (colorimetry, fluorescence and surface enhancement Raman scattering (SERS), etc.) and electrochemical (EC) methods (amperometry, potentiometry, voltammetry, electrochemical impedance spectroscopy (EIS), electrochemiluminescence (ECL) and photoelectrochemistry (PEC)) [21–25]. Among these detection methods, colorimetry offers simplicity and convenience and, until 2009, had been one of the main detection methods in PADs. The biggest advantage of paper-based colorimetric devices is that the presence of a specific analyte can be distinguished easily with the naked eye without expensive and complex instruments through the change of color. However, the colorimetric method is limited to qualitative yes/no detections and/or semi-quantitative analysis because it has several inherent disadvantages, such as narrow dynamic range, poor sensitivity and being easily interfered with by environmental light and biased by users' subjectivity. The EC method was first used as a PAD detection technique in 2009 by Dungachi et al. [38]. Generally, the analytical performances (especially sensitivity) of electrochemical paper-based analytical devices (also known as ePADs) are better than those of paper-based colorimetric analytical devices [18,23–25,28,31]. Unfortunately, the analytical performance (in particular, selectivity) of ePADs can be decreased significantly in complex matrices. Currently, the EC detection and optical detection are accounted for as the two main detection methods of PADs (as shown in Figure 1).

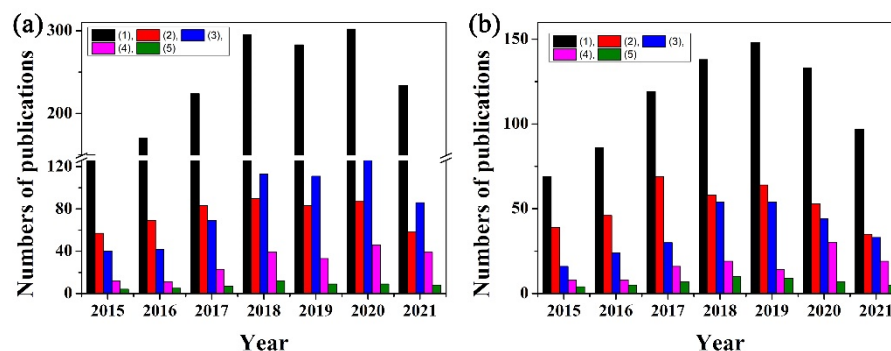


**Figure 1.** The annual publications numbers from 1 January 2015 to 30 October 2021 on the keywords: (a) (1) paper-based analytical devices and paper-based analytical devices plus (2) electrochemical, (3) colorimetric, (4) fluorescence, (5) Raman; and (b) (1) paper-based analytical devices plus nanoparticle/nanoparticles, and paper-based analytical devices plus nanoparticle or nanomaterial plus (2) electrochemical, (3) colorimetric, (4) fluorescence, (5) Raman. The data were obtained from Web of Science™.

To resolve these limitations, nanomaterials were utilized to produce selective and sensitive detection signals on PADs because nanomaterials and their composites exhibit unique physical and chemical properties (as shown in Figure 2) [26–35]. For instance, nanoparticles, including gold nanoparticles (AuNPs) and magnetic nanoparticles (MNPs), have been extensively used as signal indicators for paper-based colorimetric analytical devices [32–34]. Several AuNPs labeled lateral-flow test-strip (LFTS) immunosensors, such as human chorionic gonadotropin (HCG) and Hepatitis B surface antigen (HBsAg) colloidal gold immunoassay strips, have been clinically approved for rapid testing. Transition metal dichalcogenides (TMDs) and carbon nanomaterials, such as carbon nanotubes and graphenes, can accelerate electron transfer and increase actual electrode area when they are used as functional materials on electrode surfaces, resulting in the enhancement of the sensitivities of ePADs [18,24,31]. Fluorescent nanoparticles, such as quantum dots (QDs), carbon nanodots (CDs) and upconversion nanoparticles (UCNPs), offer new opportunities to update the assaying performance of paper-based fluorescent analytical devices in the responding time, sensitivity and selectivity because they have unique optical properties, such as tunable fluorescence color, high quantum yields, wide excitation wavelength, narrow emission band and excellent optical stability [33]. Moreover, nanomaterials have large amounts of surface-active sites as well as high surface-to-volume ratios, which sup-

port diverse functionalization with high densities of recognition units. The phenomenon further improves the detection performances of PADs. Therefore, the integration of nanomaterials with PADs enables strong quantitative capabilities of PADs and expands their applicable fields.

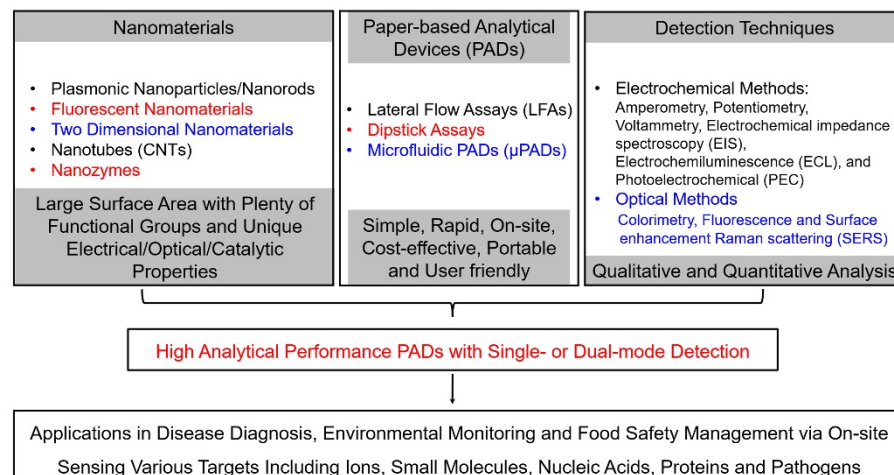


**Figure 2.** Outline of nanomaterial-based paper-based analytical devices.

Currently, great efforts are being made for improving the detection performance of PADs by using advanced materials, such as nanomaterials and their composites [33–36]. The latest reviews have extensively summarized the specific characteristics of PADs. For instance, the fabrication of nanomaterial-based colorimetric and fluorescent PADs was reviewed by Patel et al. [33]. The signal amplification strategies of nanoparticle-based lateral flow testing strips (LFTSs) have been discussed by Shirshahi and Liu [34], and Díaz-González and de la Escosura-Muñiz [35], respectively. The engineering strategies for enhancing the performance of ePAD were reviewed by Baharfar et al. [39]. Based on the detection targets, the applications of nanomaterial-based PADs have also been reviewed by several groups [27,28,36]. The purpose of this review is to introduce readers to a general overview of the recent developments regarding nanomaterial-based PADs in terms of the detection modes and their representative applications.

## 2. Nanomaterial-Enhanced Paper-Based Analytical Device

### 2.1. Electrochemical Paper-Based Analytical Devices

Due to its desirable features, such as high sensitivity, rapid response and easy miniaturization, the EC detection has gradually become one of the most commonly used detection principles for PADs. A typical immunoassay of ePAD is shown in Figure 3. After adding a drop of analyte solution on the sample zone, the analyte will bind to the detection antibody at the conjugate zone and then bind to the capture antibody at the test zone; the excess conjugates are migrated to the absorbent zone under driving by capillary action. Three electrodes (working electrode, counter electrode and reference electrode) are needed for EC analysis, and the concentration of the target analyte can be correlated to the EC response intensity of the electroactive species. The electroactive species are produced by labels catalyzed EC substrates. Dungachi et al. fabricated the first paper-based ePAD for the simultaneous determination of glucose and lactate in real samples by photolithography and screen-printing technology in 2009 [38]. Various nanomaterials and their nanocomposites have been demonstrated as powerful EC transducers and efficient electroactive label carriers in the design strategy of ePADs, which offers great improvements of the analytical performance of ePADs through increasing EC signal (e.g., current) production and decreasing background noise (i.e., enhancing signal-to-noise ratio (S/N)) (as shown in Table 1) [40–77].

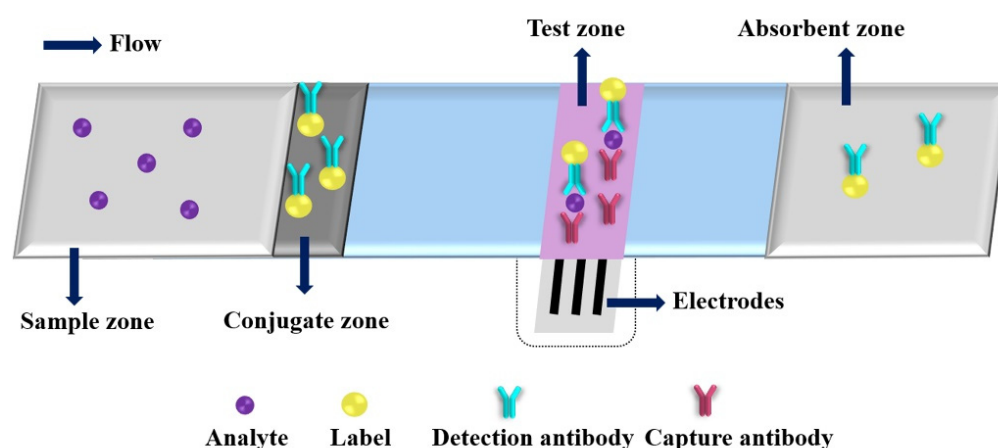


**Figure 3.** An illustration of a typical electrochemical paper-based analytical device.

Various nanoparticles, such as noble metal nanoparticles, metallic oxide nanoparticles and silica nanoparticles (SiNPs), have been extensively used to fabricate and/or modify the working electrodes of ePADs for achieving good detection performance through different methods, including directly dispersing nanoparticles in the printing ink and in situ growth, electrogeneration and drop-casting of nanoparticles on the screen-printed carbon electrodes (SPCE) [40–56]. For example, Pavithra et al. developed an ePAD for immunosensing carcinoembryonic antigen (CEA) by using AuNP working electrode, which was fabricated by directly screening printed self-made AuNP ink on the Whatman® grade 1 chromatography paper [47]. The as-developed ePAD exhibited a linear range of  $1.0 \text{ ng mL}^{-1}$  to  $100.0 \text{ ng mL}^{-1}$  with a limit of detection (LOD) of  $0.33 \text{ ng mL}^{-1}$ . The ePAD was used successfully to analyze CEA in the diluted human serum samples, demonstrating that the ePAD has good practicability. Zheng et al. developed an ePAD for ultrasensitive detection of CEA and prostate-specific antigen (PSA) by using cyclodextrin functionalized AuNPs (CD@AuNPs) and AuNPs modified paper working electrode (PWE) [40]. The CD@AuNPs exhibited mimicking properties of both glucose oxidase (GOX) and horseradish peroxidase (HRP) simultaneously, which can efficiently electrocatalytically reduce  $\text{H}_2\text{O}_2$ . The AuNPs modified PWE was constructed by in situ growth of AuNPs on the surfaces of cellulose fibers of paper. Taking advantage of the high conductivity of AuNP modified PWE and good catalytic activity of CD@AuNPs, the as-developed ePAD exhibited wide linear ranges ( $0.005$  to  $100 \text{ ng mL}^{-1}$  (CEA) and  $0.002$  to  $40 \text{ ng mL}^{-1}$  (PSA)), low LODs ( $0.002 \text{ ng mL}^{-1}$  (CEA)  $0.001 \text{ ng mL}^{-1}$  (PSA) and high stability (retaining 90% of the initial responses after stored at  $4 \text{ }^\circ\text{C}$  for 15 days). The ePAD was used to detect CEA and PSA in spiked human serum samples, and satisfactory recoveries (in the range of 100.4% to 109.2% for CEA and in the range of 100.9% to 114.0% for PSA) were obtained, indicating that the ePAD has a great potential application of detecting CEA and PSA in clinical samples. Pinyorosphatum et al. developed an ePAD for detection of C-reactive protein (CRP) through electrodeposited AuNPs on SPCE, followed by the self-assembly of PMPC-SH on AuNP surface [41]. In the presence of CRP and  $\text{Ca}^{2+}$ , the current of ePAD was decreased by increasing the concentration of CRP, while  $[\text{Fe}(\text{CN})_6]^{3-/4-}$  was used as the electrochemical probe. The as-developed ePAD exhibited a linear range of  $5$  to  $5000 \text{ ng}\cdot\text{mL}^{-1}$  with an LOD of  $1.6 \text{ ng}\cdot\text{mL}^{-1}$ , which was applied successfully to detect CRP in the certified human serum samples. De França developed an ePAD for detection of dopamine through drop-casting CdSe/CdS magic-sized QDs (MSQDs) on the graphite working electrode (5 mm in diameter), which was drawn on chromatography paper by 6B grade pencil [52]. After being decorated by  $10 \mu\text{g}$  MSQDs, the peak current was enhanced ca. 46% in comparison with that of bare electrode, besides a decrease in the charge transfer resistance and increase in the electroactive area of the sensor. The as-developed ePAD exhibited excellent analytical performance, including low LOD ( $96 \text{ nmol L}^{-1}$ ), good stability (within a period of 7 days without major variations of peak current), repeatability (ca. 2.85% relative standard de-

variation (RSD) and reproducibility (ca. 7.2% RSD). The ePAD was employed successfully for sensing dopamine in human blood serum samples with recovery rates between 95.2% and 102.6%. Because of their high catalytic activity, nanomaterials can also be used as active probe for developed ECL PAD [54–56]. For instance, Huang et al. developed an auto-cleaning ECL PAD for detection of  $\text{Ni}^{2+}$  and  $\text{Hg}^{2+}$  through using superior peroxidase-like activity of cubic  $\text{Cu}_2\text{O}$ -Au nanoparticles and a large specific surface area and excellent conductivity of silver nanoparticles (AgNPs) [55]. The cubic  $\text{Cu}_2\text{O}$ -Au nanoparticles can catalyze  $\text{H}_2\text{O}_2$  to generate reactive oxygen species, promoting the luminescence of N-(4-Aminobutyl)-N-ethylisoluminol (ABEI). The as-developed ECL PAD exhibited wide linear ranges ( $10 \text{ nmol L}^{-1}$  to  $0.2 \text{ mmol L}^{-1}$  ( $\text{Ni}^{2+}$ ) and  $10 \text{ pmol L}^{-1}$  to  $1 \text{ } \mu\text{mol L}^{-1}$  ( $\text{Hg}^{2+}$ )) and low LODs ( $3.1 \text{ nmol L}^{-1}$  ( $\text{Ni}^{2+}$ ) and  $3.8 \text{ pmol L}^{-1}$  ( $\text{Hg}^{2+}$ )), which was used successfully to detect  $\text{Ni}^{2+}$  and  $\text{Hg}^{2+}$  in the spiked lake water.

As transduction materials, carbon nanomaterials, including single-walled carbon nanotubes (SWCNTs), multi-walled carbon nanotubes (MWCNTs) and different types of graphene materials, have been getting great attention in the ePAD fabrication because they have high surface area, excellent electrical conductivity and rich surface-chemical properties [57–73]. For instance, Valentine et al. found that the device-to-device reproducibility and current intensity of ePAD can be efficiently improved through formation of MWCNT network in the porous structures of paper [58]. Tran et al. developed an ePAD for non-enzymatic detection of glucose through the deposition of the SWCNT layer on wax-printed nitrocellulose (NC) membrane [59]. The SWCNT electrode exhibits high conductivity with an average resistivity of less than  $100 \text{ } \Omega/\text{sq}$  and excellent mechanical property. After modification of the SWCNT electrode by AuNPs, the as-developed ePAD exhibited excellent glucose detection performance, including good reproducibility (RSD < 8%) and high sensitivity ( $240 \text{ } \mu\text{A}/\text{mM cm}^2$ ), which was used successfully to determine glucose in Coke. Pungjunun et al. developed an origami-based ePAD for sensing  $\text{NO}$  and  $\text{NO}_2$  (as  $\text{NO}_x$ ) by using a screen-printed graphene electrode modified with copper nanoparticles (CuNP/SPGE) [64]. Because of the good catalytic property of CuNP towards the EC conversion of  $\text{NO}_x$  and excellent conductivity of graphene, the as-developed ePAD exhibited high selectivity, low LODs ( $0.23 \text{ vppm}$  and  $0.03 \text{ vppm}$  with exposure times of 25 min and 1 h, respectively), good reproducibility (RSD < 5.1%) and long lifetime (>30 days). The ePAD was applied to detect  $\text{NO}_x$  in air and exhaust gases from cars, and satisfactory results were obtained. Cai group has been developed a series of ePADs for detection of various biomarkers, including CEA and neuron-specific enolase (NSE), by using amino functional graphene (NG)-Thionin (THI)-AuNPs nanocomposites modified SPCEs [66,67]. Integration of SiNPs modified paper microzones with reduced graphene (RG) modified SPCE, Scala-Benuzzi et al. developed an ePAD for the quantitative determination of ethinylestradiol (EE2) in water samples through capturing EE2 by the immobilized anti-EE2 specific antibodies on the paper microzones, subsequently releasing the adsorbed EE2 by adding a diluted solution of sulfuric acid and detecting the desorbed EE2 by Osteryoung square wave voltammetry (OSWV) [69]. The as-developed ePAD exhibited excellent analytical performance, including wide linear range ( $0.5$  to  $120 \text{ ng L}^{-1}$ ), low LOD ( $0.1 \text{ ng L}^{-1}$ ) good recovery values (from 97% to 104%) and good reproducibility (RSD < 4.9%). There are no significant differences were found between the results of ePAD and the results of spectrophotometric immunoassay, when two methods were used for the quantification of EE2 in river water samples and spiked water samples.

**Table 1.** The typical nanomaterial-enhanced ePADs for sensing various analytes.

Nanomaterials	Modification Methods	Electrochemical Method	Analytes	Linear Ranges	Limit of Detection	Real Samples	Recovery	Ref.
AuNPs	In situ growth	DPV	CEA and PSA	$5 \times 10^{-3}$ to $100 \text{ ng mL}^{-1}$ (CEA) and $2 \times 10^{-3}$ to $40 \text{ ng mL}^{-1}$ (PSA)	$2 \times 10^{-3} \text{ ng mL}^{-1}$ (CEA) $1 \times 10^{-3} \text{ ng mL}^{-1}$ (PSA)	Human serum	-	[40]
AuNPs	Electrodeposition	DPV	CRP	$5$ to $5 \times 10^3 \text{ ng mL}^{-1}$	$1.6 \text{ ng mL}^{-1}$	Certified human serum	-	[41]
AuNPs	Electrodeposition	DPV	EGFR	$0.5$ to $500 \text{ nmol L}^{-1}$	$0.167 \text{ nmol L}^{-1}$	Saliva samples	-	[42]
AuNPs	Drop-casting	DPV	H1047R (A3140G) missense mutation in exon 20	-	$5 \text{ nmol L}^{-1}$ (signal on) and $6 \text{ nmol L}^{-1}$ (signal off)	-	-	[43]
AuNPs	Electrodeposition	Impedimetry	miRNA 155	$0$ to $4 \times 10^3 \text{ ng mL}^{-1}$	$6.9 \times 10^2 \text{ ng mL}^{-1}$ ( $93.4 \text{ nmol L}^{-1}$ )	Fetal bovine serum	-	[44]
AuNPs	Drop-casting	SWASV	$\text{Hg}^{2+}$	$5$ to $200 \text{ ng mL}^{-1}$	$2.5 \text{ ng mL}^{-1}$	Drinking water	95% to 104%	[45]
Poly (N-vinylpyrrolidone) AuNPs	Screen-printing	Chronoamperometry	Glucose	$1 \times 10^4$ to $1.5 \times 10^6 \text{ nmol L}^{-1}$	$2.6 \times 10^4 \text{ nmol L}^{-1}$	-	-	[46]
Poly (N-vinylpyrrolidone) AuNPs	Screen-printing	DPV	CEA	$1$ to $100 \text{ ng mL}^{-1}$	$0.33 \text{ ng mL}^{-1}$	Diluted human serum	99.58% to 102.50%	[47]
Pd decoration of Cu/Co-doped $\text{CeO}_2$ (CuCo- $\text{CeO}_2$ -Pd) nanospheres and urchin-like AuNPs	In situ growth	DPV	Amyloid- $\beta$	$1 \times 10^{-3}$ to $100 \text{ nmol L}^{-1}$	$5 \times 10^{-5} \text{ nmol L}^{-1}$	Artificial cerebrospinal fluid and human serum	99% to 100.5%	[48]
N-CDs, $\text{TiO}_2$ NPs and Pt NPs	Drop-casting	PEC	CEA	$2 \times 10^{-3}$ to $200 \text{ ng mL}^{-1}$	$1.0 \times 10^{-3} \text{ ng mL}^{-1}$	Living MCF-7 cells	-	[49]
$\text{TiO}_2$ nanosheets and $\text{CeO}_2$ NPs	In situ growth of $\text{TiO}_2$ nanosheets and drop-casting of $\text{CeO}_2$ NPs	PEC	Thrombin	$2 \times 10^{-5}$ to $0.1 \text{ nmol L}^{-1}$	$6.7 \times 10^{-6} \text{ nmol L}^{-1}$	Human serum	-	[50]
CdSe/CdS magic-sized QDs	Drop-casting	DPV	Dopamine	$500$ to $1.5 \times 10^4 \text{ nmol L}^{-1}$	$96 \text{ nmol L}^{-1}$	Human serum	95.2% to 102.6%	[51]
ZnO NPs	Drop-casting	SWV	Picric acid	$4 \times 10^3$ to $6 \times 10^4 \text{ nmol L}^{-1}$	$4.04 \times 10^3 \text{ nmol L}^{-1}$	Tap water, lake water	92.3% to 98.9%	[52]

Table 1. Cont.

Nanomaterials	Modification Methods	Electrochemical Method	Analytes	Linear Ranges	Limit of Detection	Real Samples	Recovery	Ref.
Molecularly imprinted polymer coated Fe <sub>3</sub> O <sub>4</sub> @Au@SiO <sub>2</sub> NPs	Drop-casting	LSV	Serotonin	10 to 10 <sup>6</sup> nmol L <sup>-1</sup>	2 nmol L <sup>-1</sup>	Pharmaceutical capsules and urine samples	100% to 111%	[53]
Patchy gold coated Fe <sub>3</sub> O <sub>4</sub> nanospheres	-	ECL	CEA	1 × 10 <sup>-4</sup> ng mL <sup>-1</sup> to 15 ng mL <sup>-1</sup>	3 × 10 <sup>-5</sup> ng mL <sup>-1</sup>	Human serum	-	[54]
Cubic Cu <sub>2</sub> O-Au NPs and AgNPs	In situ growth (AgNPs)	ECL	Ni <sup>2+</sup> and Hg <sup>2+</sup>	10 to 2 × 10 <sup>5</sup> nmol L <sup>-1</sup> (Ni <sup>2+</sup> ) and 1 × 10 <sup>-2</sup> nmol L <sup>-1</sup> to 1 × 10 <sup>3</sup> nmol L <sup>-1</sup> (Hg <sup>2+</sup> )	3.1 nmol L <sup>-1</sup> (Ni <sup>2+</sup> ) and 3.8 × 10 <sup>-3</sup> nmol L <sup>-1</sup> (Hg <sup>2+</sup> )	Lake water	96.4% to 101.6% (Ni <sup>2+</sup> ) and 96.0% to 104.0% (Hg <sup>2+</sup> )	[55]
DNA-functionalized PtCu nanoframes	-	ECL	Streptavidin	1 × 10 <sup>-4</sup> nmol L <sup>-1</sup> to 100 nmol L <sup>-1</sup>	3.34 × 10 <sup>-5</sup> nmol L <sup>-1</sup>	Human serum	98.4% to 106.5%	[56]
SWCNTs	Vacuum filtration	CV	Glucose	5 × 10 <sup>-5</sup> to 1 × 10 <sup>7</sup> nmol L <sup>-1</sup>	1.48 × 10 <sup>5</sup> nmol L <sup>-1</sup>	Coke	97.3% to 105%	[59]
Graphene	Screen-printing	DPV	Oxytetracycline	1 to 200 ng mL <sup>-1</sup>	0.33 ng mL <sup>-1</sup>	Milk, honey and shrimp	-	[60]
Graphene	Screen-printing	DPV	Hepatitis B virus DNA	5 × 10 <sup>-2</sup> to 100 nmol L <sup>-1</sup>	1.45 × 10 <sup>-3</sup> nmol L <sup>-1</sup>	Plasmid constructs	-	[61]
Graphene	Screen-printing	SWV	Salivary thiocyanate	2.5 × 10 <sup>4</sup> to 7 × 10 <sup>5</sup> nmol L <sup>-1</sup>	6 × 10 <sup>3</sup> nmol L <sup>-1</sup>	Human saliva	-	[62]
Graphene	Drop-casting	DPV	ATP	3 × 10 <sup>2</sup> to 4.5 × 10 <sup>5</sup> nmol L <sup>-1</sup>	80 nmol L <sup>-1</sup>	Human serum and cell lysates	95.4% to 104.2%	[63]
Graphene and CuNPs	Screen-printing (graphene) and in situ growth CuNPs	DPV	NOx	0 to 150 vppm	0.23 vppm	Ambient indoor and outdoor air, and exhaust gases	-	[64]
Graphene and AuNPs	Drop-casting (graphene) and label (AuNPs)	DPV	Pseudopodium-enriched atypical kinase one	1 × 10 <sup>-2</sup> to 1 × 10 <sup>3</sup> ng mL <sup>-1</sup>	1 × 10 <sup>-2</sup> ng mL <sup>-1</sup>	Human serum	103% to 104%	[65]
(NH <sub>2</sub> -G)/Thi/AuNPs nanocomposites	Drop-casting	DPV	CEA	5 × 10 <sup>-2</sup> to 500 ng mL <sup>-1</sup>	1 × 10 <sup>-2</sup> ng mL <sup>-1</sup>	Human serum	-	[66]
(NH <sub>2</sub> -G)/Thi/AuNPs nanocomposites	Drop-casting	DPV	CEA and NSE	1 × 10 <sup>-2</sup> to 500 ng mL <sup>-1</sup> for CEA and 5 × 10 <sup>-2</sup> to 500 ng mL <sup>-1</sup> for NSE	2 × 10 <sup>-3</sup> ng mL <sup>-1</sup> for CEA and 1 × 10 <sup>-2</sup> ng mL <sup>-1</sup> for NSE	Human serum	-	[67]

Table 1. Cont.

Nanomaterials	Modification Methods	Electrochemical Method	Analytes	Linear Ranges	Limit of Detection	Real Samples	Recovery	Ref.
Reduced graphene	Screen-printing and in situ EC reduction	Amperometry	Claudin 7 and CD81	$2 \times 10^{-3}$ to $1 \text{ ng mL}^{-1}$ (Claudin 7) and $0.01$ to $10 \text{ ng mL}^{-1}$ (CD81)	$4 \times 10^{-4} \text{ ng mL}^{-1}$ (Claudin 7) and $3 \times 10^{-3} \text{ ng mL}^{-1}$ (CD81)	Plasma of breast cancer patients	-	[68]
Reduced graphene	Drop-casting and EC reduction	SWV	Ethinylestradiol	$5 \times 10^{-4}$ to $0.12 \text{ ng mL}^{-1}$	$1 \times 10^{-4} \text{ ng mL}^{-1}$	River water	97.5% to 103.7%	[69]
Graphene QDs	Drop-casting	SWV	UA and creatinine	$10$ to $3 \times 10^3 \text{ nmol L}^{-1}$	$8.4 \text{ nmol L}^{-1}$ (UA) and $3.7 \text{ nmol L}^{-1}$ (Creatinine)	Human urine	98.9% to 101.5%	[70]
GO	Drop-casting	SWV	CRP, cTnI and PCT	$1$ to $1 \times 10^5 \text{ ng mL}^{-1}$ (CRP), $1 \times 10^{-3}$ to $250 \text{ ng mL}^{-1}$ (cTnI), $5 \times 10^{-4} \text{ ng mL}^{-1}$ to $250 \text{ ng mL}^{-1}$ (PCT)	$0.38 \text{ ng mL}^{-1}$ (CRP), $1.6 \times 10^{-4} \text{ ng mL}^{-1}$ (cTnI) and $2.7 \times 10^{-4} \text{ ng mL}^{-1}$ (PCT)	Human serum	-	[71]
RGO and cysteine AuNPs	Drop-casting (RGO) and electrodeposition (AuNPs)	Chronoamperometry	IL-8	$1 \times 10^{-3}$ to $9 \times 10^{-3} \text{ ng mL}^{-1}$	$5.89 \times 10^{-4} \text{ ng mL}^{-1}$	-	-	[72]
(NH <sub>2</sub> -GO)/Thi/AuNPs	Screen-printing	DPV	EGFR	$5 \times 10^{-2}$ to $200 \text{ ng mL}^{-1}$	$5 \times 10^{-2} \text{ ng mL}^{-1}$	Human serum	-	[73]
rGO/Thi/S-AuNP/Chi	Drop-casting	Amperometry	17 $\beta$ -E2	$1 \times 10^{-2}$ to $100 \text{ ng mL}^{-1}$	$1 \times 10^{-2} \text{ ng mL}^{-1}$	Human serum	-	[74]
Cobalt-MOF	In situ growth	Amperometry	Glucose	$8 \times 10^5$ to $1.6 \times 10^7 \text{ nmol L}^{-1}$	$1.5 \times 10^5 \text{ nmol L}^{-1}$	Serum, Urine and Saliva	87.2% to 108.6%	[75]
Pd@hollow Zn/Co core-shell ZIF67/ZIF8 NPs	Drop-casting	DPV	PSA	$5 \times 10^{-3} \text{ ng mL}^{-1}$ to $50 \text{ ng mL}^{-1}$	$7.8 \times 10^{-4} \text{ ng mL}^{-1}$	-	-	[76]
Ni-MOFs/AuNPs/MWCNTs/PVA	Vacuum filtration (MWCNT/PVA) and drop-casting (Ni-MOFs/AuNPs)	DPV	HIV DNA	$10$ to $1 \times 10^3 \text{ nmol L}^{-1}$	$0.13 \text{ nmol L}^{-1}$	Human serum	95.5% to 103.8%	[77]

CV: cyclic voltammetry; SWV: square wave voltammetry; ECL: electrochemical luminescence; PEC: photoelectrochemical; DPV: differential pulse voltammetry; EIS: electrochemical impedance spectroscopy; ASV: anodic stripping voltammetry; LSV: linear-sweep voltammetry; SWASV: square wave anodic stripping voltammetry; 2D: two dimension; 3D: three dimension; NPs: nanoparticles; AuNPs: gold nanoparticles; CDs: carbon dots; N-CDs: nitrogen-doped carbon dots; QDs: quantum dots; AgNPs: silver nanoparticles; SWCNTs: single-walled carbon nanotubes; MWCNTs: multiple-walled carbon nanotubes; MOFs: metal-organic frameworks; Ni-MOFs: nickel metal-organic frameworks; CuNPs: copper nanoparticles; (NH<sub>2</sub>-G)/Thi/AuNPs: amino functionalized graphene/thionine/gold nanoparticles nanocomposites; RGO: reduced graphene oxide; GO: graphene oxide; rGO/Thi/S-AuNP/Chi: amino redox graphene/thionine/streptavidin-modified gold nanoparticles/chitosan; ZIF: zeolite imidazole ester framework material; PVA: polyvinyl alcohol; CEA: carcinoembryonic antigen; PSA: prostate-specific antigen; CRP: C-reactive protein; EGFR: epidermal growth factor receptor; NSE: neuron-specific enolase; ATP: adenosine triphosphate; UA: uric acid; IL-8: interleukin 8; cTnI: cardiac troponin I; PCT: procalcitonin.

The unique features of metal-organic frameworks (MOFs), including high porosity, tunable framework structures, large surface areas and multiple functionalities, make them extremely attractive for improving the detection performance of biosensors [78,79]. Recently, MOFs and their nanocomposites have been used for developing ePAD with excellent detection performance [75–77]. Wei et al. fabricated a cobalt-MOF (Co-MOF) modified carbon cloth/paper (CC/Paper) hybrid button-based PAD (Co-MOF/CC PAD) for nonenzymatic quantitative EC detection of glucose through in situ growth of Co-MOF on CC [75]. As a typical nanozyme, the environment tolerance of Co-MOFs is much better than that of natural enzyme, which can increase significantly the stability of ePAD. Densely grown Co-MOF on CC can maximize its catalytic sites, resulting in high sensitivity of ePAD. The Co-MOF/CC PAD exhibits linear range from 0.8 mmol L<sup>-1</sup> to 16 mmol L<sup>-1</sup> with an LOD of 0.15 mmol L<sup>-1</sup> and maintains at a stable detection performance in 60 days, and then gradually decreased to about 60% after 120 days. The ePAD was used successfully to determine glucose in multiple body fluids, including serum, urine and saliva. Lu et al. developed an ePAD-based DNA hybridization for detection of human immunodeficiency virus (HIV) DNA by using the nickel MOF (Ni-MOF) composite/AuNPs/CNTs/polyvinyl alcohol (Ni–Au composite/CNT/PVA) paper electrode as working electrode and methylene blue (MB) as a redox indicator [77]. The CNT/PVA were deposited on the cellulose membrane by vacuum filtration, and Ni–Au composites were loaded on CNT/PVA film by the drop-casting method. The Ni–Au composite/CNT/PVA film electrode has large specific surface area and conjugated  $\pi$ -electron system, which makes a higher loading of the single-stranded DNA probe than that of CNT/PVA film electrode. The phenomenon improves the sensitivity for detecting target DNA. The ePAD exhibited excellent sensing performance with a wide linear range of 10 nmol L<sup>-1</sup> to 1  $\mu$ mol L<sup>-1</sup>, a low LOD of 0.13 nmol L<sup>-1</sup>, good selectivity against one-base mismatch DNA sequences and excellent stability after 20 days of storage. The target HIV DNA was detected successfully even in complex serum samples by the as-developed ePAD.

## 2.2. Colorimetric Paper-Based Analytical Devices

Colorimetric detection is the most common method in PADs. Figure 4 shows a typical schematic of colorimetric test strip. Generally, the test strip includes five functional zones: sample, conjugate, test, control and absorbent zones. Under the analyte solution migration, conjugates will capture the analyte with detection antibody at conjugate zone, and then the conjugates and analyte bind to the capture antibody at test zone, the excess conjugates are migrated to the control zone conjugate with secondary antibody. After finishing the reaction, the ImageJ is usually used for the collecting colorimetric signals of the test and control lines. Up to now, various kinds of nanomaterials are used as colorimetric labels. The nanomaterial-based colorimetric PADs have been extensively used for detection of various targets (as shown in Table 2) [43,80–112]. Plasmonic nanoparticles, such as AuNPs and AgNPs, are extremely useful indicators for the fabrication of colorimetric PADs because of their strong local surface plasmon resonance (SPR) bands [80]. Moreover, multiple, simultaneous tests can be rapidly performed with low sample consumption by incorporating these surface-modified AuNPs into a PADs that can be read using just a smartphone. For example, Díaz-Amaya et al. developed a  $\mu$ PAD for multiplexed aptamer-based detection of analytical targets through a salt-induced aggregation of single strand DNA (ssDNA) functionalized polyethyleneimine (PEI) encapsulation of gold-decorated polystyrene (PS) core particles (ssDNA-PEI-Au-PS) [85]. The net positive charge of the PEI layer avoids the direct interaction of metallic ions and ssDNAs with the AuNPs, which provides ideal conditions for controlled induction of aggregation of AuNPs on the test zones of  $\mu$ PAD, resulting in high sensitivity, selectivity and reproducibility (RSD = 5.69%). Using a smartphone as detector, the analytical performance of as-proposed  $\mu$ PAD was demonstrated by multiplexed detection of Hg<sup>2+</sup> and As<sup>3+</sup> with low LODs (1  $\mu$ g mL<sup>-1</sup>) and high specificity ( $p > 0.05$ ) versus different interferent ions (Ca<sup>2+</sup>, Fe<sup>2+</sup>, Mg<sup>2+</sup> and Pb<sup>2+</sup>). The authors provided a universal idea for fabricating  $\mu$ PAD with the capability of multiplex and

quantitative colorimetric detection. Monisha et al. reported a PAD with AgNPs for on-site determination of  $\text{Hg}^{2+}$  from environmental water samples by inkjet-printing polyvinyl pyrrolidone (PVP) stabilized AgNPs on Whatman<sup>®</sup> grade 1 chromatography paper [96]. In the presence of  $\text{Hg}^{2+}$ , the color of AgNP is changed from yellow to colorless because of the oxidation of AgNPs into  $\text{Ag}^+$  ions on the paper substrate. The as-proposed PAD exhibited the linear range from 40 to 1200  $\text{ng mL}^{-1}$  with LOD of 10  $\text{ng mL}^{-1}$ , and was used successfully for quantitative detection of  $\text{Hg}^{2+}$  in different types of water samples collected from river, tube well, pond, coal mines and industrial waste. This approach could be used to determine  $\text{Hg}^{2+}$  in other real samples, such as biological and vegetable samples. Recently, Mettakoopitak et al. developed an uncomplicated, affordable and environmentally friendly method for fabrication of  $\mu\text{PAD}$  by screen-printing biodegradable polycaprolactone (PCL) as high-resolution hydrophobic barriers [98]. The proposed method can produce as narrow as  $510 \pm 40 \mu\text{m}$  hydrophilic channel and  $490 \pm 30 \mu\text{m}$  hydrophobic edge, respectively. The as-developed method was used successfully to fabricate  $\mu\text{PADs}$  for detection of  $\text{Cr}^{3+}$  and  $\text{Cl}^-$  with high selectivity. For  $\text{Cr}^{3+}$  analysis, the  $\mu\text{PADs}$  achieved a linear range of 50.0 to 1000.0  $\text{ng mL}^{-1}$  with an LOD of 15.0  $\text{ng mL}^{-1}$ , when AgNPs were used as the colorimetric probe. Integration of nanoparticle as color indicator and PCL screen-printing could provide a simple and environmentally friendly method for fabricating  $\mu\text{PADs}$  with high analytical performance, which are ultimately utilized in wide-ranging applications.

In addition, the AuNPs can also serve as carriers for the simultaneous immobilization of different biomolecules (e.g., antibodies, DNA and aptamers) with an abundant number of biorecognition elements or optical/electrochemical tags on their surfaces to provide more binding sites or signal amplification of analyte for a single recognition reaction. Furthermore, different antibodies can be easily introduced to the AuNP surface via electrostatic interactions to provide highly specific recognition sites for biomolecular sensing, resulting in simplify the PAD fabrication procedure. Huang et al. reported a highly sensitive colorimetric PAD for detection of PSA by using AuNPs labeled with biotinylated poly(adenine) ssDNA sequences and streptavidin-HRP for enzymatic signal enhancement [87]. The as-proposed PAD was able to detect as low as 10  $\text{pg mL}^{-1}$  PSA in a test that could be completed in as little as 15 min.

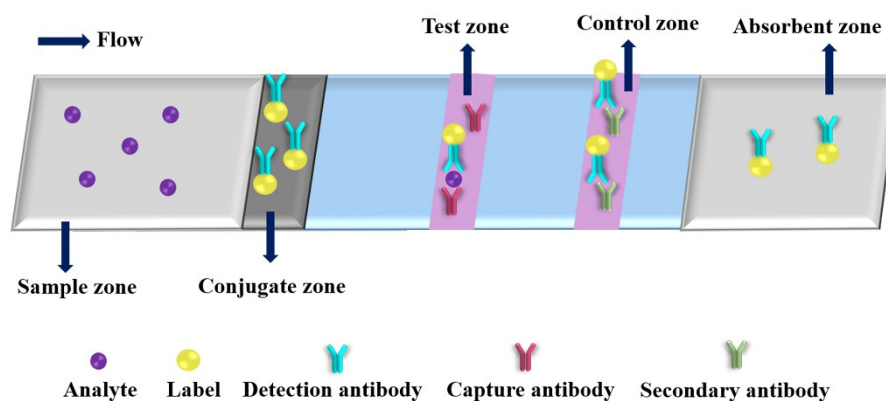


**Figure 4.** An illustration of a typical colorimetric paper-based analytical device.

**Table 2.** The typical nanomaterial-enhanced colorimetric PADs for sensing various analytes.

Nanomaterials	Analytes	Linear Ranges	Limit of Detection	Real Samples	Recovery	Ref.
AuNPs	Gallic acid	$1 \times 10^4$ to $1 \times 10^6$ nmol L <sup>-1</sup>	$1 \times 10^3$ nmol L <sup>-1</sup>	Tea	85.2% to 93.1%	[80]
Avidin functionalized AuNPs	Ig G	-	300 ng mL <sup>-1</sup>	-	-	[81]
Citrate stabilized AuNPs	Melamine	100 to $10^6$ ng mL <sup>-1</sup>	100 ng mL <sup>-1</sup>	Milk	-	[82]
Citrate stabilized AuNPs	NADH	-	$1.25 \times 10^4$ nmol L <sup>-1</sup>	Cell Lysate	-	[83]
Aspartic acid modified AuNPs	Cysteine	$9.99 \times 10^4$ to $9.987 \times 10^5$ nmol L <sup>-1</sup>	$1 \times 10^3$ nmol L <sup>-1</sup>	Human plasma	99.2% to 101.1%	[84]
ssDNA-PEI-Au-PS	Hg <sup>2+</sup> and As <sup>3+</sup>	0 to $3 \times 10^4$ ng mL <sup>-1</sup>	$1 \times 10^3$ ng mL <sup>-1</sup>	River water	96.2% to 116.7%	[85]
ssDNA functionalized AuNPs	Tuberculosis DNA	$1.95 \times 10^{-2}$ to 19.5 ng mL <sup>-1</sup>	$1.95 \times 10^{-2}$ ng mL <sup>-1</sup>	Infected tissue	-	[86]
ssDNA functionalized AuNPs	PSA	-	$1 \times 10^{-2}$ ng mL <sup>-1</sup>	Human serum	-	[87]
Antibody functionalized AuNPs	Ig G	-	284.52 ng mL <sup>-1</sup>	Whole blood	-	[88]
Antibody functionalized AuNPs	Yersinia Pestis	-	$2.5 \times 10^{-2}$ ng mL <sup>-1</sup>	-	-	[89]
Antibody functionalized AuNPs	Influenza A H1N1 and H3N2 viruses	-	$2.7 \times 10^3$ pfu/assay for H1N1 detection and $2.7 \times 10^4$ pfu/assay for H3N2 detection	Cell lysate	-	[90]
Antibodies functionalized AuNRs	sIL-2R	1 to $6.25 \times 10^3$ ng mL <sup>-1</sup>	1.0 ng mL <sup>-1</sup>	Mouse serum	93% to 109%	[91]
Antibodies functionalized AuNRs	CRP	50 to $1 \times 10^4$ ng mL <sup>-1</sup>	1.3 ng mL <sup>-1</sup>	Human plasma	-	[92]
Co(II) catalyst, secondary antibody, luminol multifunctionalized AuNPs	H-FABP, cTnI and copeptin	$1 \times 10^{-4}$ to $1 \times 10^3$ ng mL <sup>-1</sup> , $5 \times 10^{-4}$ to $1 \times 10^3$ ng mL <sup>-1</sup> and $1 \times 10^{-3}$ to $1 \times 10^6$ ng mL <sup>-1</sup> for H-FABP, cTnI and copeptin	$6 \times 10^{-5}$ ng mL <sup>-1</sup> , $3 \times 10^{-4}$ ng mL <sup>-1</sup> and $4 \times 10^{-4}$ ng mL <sup>-1</sup> for H-FABP, cTnI and copeptin	Human serum	94% to 108%	[93]

Table 2. Cont.

Nanomaterials	Analytes	Linear Ranges	Limit of Detection	Real Samples	Recovery	Ref
Cu/Co-doped CeO <sub>2</sub> (CuCo-CeO <sub>2</sub> -Pd) nanospheres and urchin-like AuNPs	Amyloid- $\beta$	$1 \times 10^{-2}$ to 100 nmol L <sup>-1</sup>	$5 \times 10^{-4}$ nmol L <sup>-1</sup>	Artificial cerebrospinal fluid (aCSF) and human serum	99% to 100.5%	[48]
Gold nanostars	Glucose	0 to $2 \times 10^7$ nmol L <sup>-1</sup>	$1.4 \times 10^6$ nmol L <sup>-1</sup>	-	-	[94]
PVP stabilized AgNPs	Nitrite	10 to $5 \times 10^3$ nmol L <sup>-1</sup> and $10^4$ to $3.2 \times 10^6$ nmol L <sup>-1</sup>	$8.5 \times 10^{-2}$ nmol L <sup>-1</sup>	Tap, river and lake water	95.6% to 101.9%	[95]
PVP stabilized AgNPs	Hg <sup>2+</sup>	40 to $1.2 \times 10^3$ ng mL <sup>-1</sup>	10 ng mL <sup>-1</sup>	Tube well, river pond water, industrial waste and coal mine water	92.5% to 96.0%	[96]
PVP stabilized AgNPs	Ascorbic acid	$1 \times 10^6$ to $4 \times 10^6$ nmol L <sup>-1</sup>	$8.28 \times 10^4$ nmol L <sup>-1</sup>	Vitamin C tablet and artificial juice	-	[97]
Citrate stabilized AgNPs	Cr <sup>3+</sup> and Cl <sup>-</sup>	50 to $1 \times 10^3$ ng mL <sup>-1</sup> (Cr <sup>3+</sup> ) and $1 \times 10^4$ to $5 \times 10^5$ ng mL <sup>-1</sup> (Cl <sup>-</sup> )	15 ng mL <sup>-1</sup> (Cr <sup>3+</sup> ) and $1 \times 10^4$ ng mL <sup>-1</sup> (Cl <sup>-</sup> )	Instant noodle seasoning	-	[98]
Citrate stabilized AgNPs	Hg <sup>2+</sup>	1 to 4 ng mL <sup>-1</sup>	0.86 ng mL <sup>-1</sup>	River water	98.9% to 101%	[99]
Achillea Wilhelmsii extract coated AgNPs	Hg <sup>2+</sup>	$1 \times 10^3$ to $7 \times 10^5$ nmol L <sup>-1</sup>	300 nmol L <sup>-1</sup>	River, well and lake water	-	[100]
Citrate capped Cu@Ag core@shell NPs	Phenthoate	50 to $1.5 \times 10^3$ ng mL <sup>-1</sup>	15 ng mL <sup>-1</sup>	Pond and river water, cucumber and potato	92.6% to 97.4%	[101]
DNA-templated Ag/Pt NCs	miRNA21	$1 \times 10^{-3}$ to 0.7 nmol L <sup>-1</sup>	$6 \times 10^{-4}$ nmol L <sup>-1</sup>	Human urine	93.8% to 106.0%	[102]
ssDNA functionalized PtNPs	miRNAs	$1 \times 10^{-2}$ to 100 nmol L <sup>-1</sup>	$8.5 \times 10^{-3}$ nmol L <sup>-1</sup> (miRNA21)	Human Serum	86.2% to 112.2%	[103]
Pd NPs/meso-C	H <sub>2</sub> O <sub>2</sub>	$5 \times 10^3$ to $3 \times 10^5$ nmol L <sup>-1</sup>	$1 \times 10^3$ nmol L <sup>-1</sup>	Commercial milk	100.9% to 109.7%	[104]
ZnONRs	Glucose and UA	Glucose ( $1 \times 10^4$ to $1 \times 10^7$ nmol L <sup>-1</sup> ) and uric acid ( $1 \times 10^4$ to $5 \times 10^6$ nmol L <sup>-1</sup> )	$3 \times 10^3$ nmol L <sup>-1</sup> for glucose and $4 \times 10^3$ nmol L <sup>-1</sup> for uric acid	Human serum and urine	89% to 109%	[105]

Table 2. Cont.

Nanomaterials	Analytes	Linear Ranges	Limit of Detection	Real Samples	Recovery	Ref
Cr <sub>2</sub> O <sub>3</sub> -TiO <sub>2</sub> nanocomposites	H <sub>2</sub> O <sub>2</sub>	5 to 1 × 10 <sup>5</sup> nmol L <sup>-1</sup>	3 nmol L <sup>-1</sup>	Tap water, milk and fetal bovine serum (FBS) albumin	95.8% to 98%	[106]
Mn-ZnS QDs	Glyphosate	5 to 5 × 10 <sup>4</sup> ng mL <sup>-1</sup>	2 ng mL <sup>-1</sup>	Whole grain	80.6% to 119.9%	[107]
N-CDs	H <sub>2</sub> O <sub>2</sub>	5 × 10 <sup>4</sup> to 1 × 10 <sup>7</sup> nmol L <sup>-1</sup>	1.4 × 10 <sup>4</sup> nmol L <sup>-1</sup>	Human plasma	91.0% to 113.0%	[108]
CDs@Eu/GMP ICPs	Cerebral acetylcholinesterase	0.1 mU mL <sup>-1</sup> to 60 mU mL <sup>-1</sup>	0.033 mU mL <sup>-1</sup>	Brain tissues and cerebral fluid	-	[109]
Carbon nitride nanoparticles	Tetracycline	800 to 4 × 10 <sup>5</sup> nmol L <sup>-1</sup>	120 nmol L <sup>-1</sup>	Shrimp samples and river water	98.7% to 102.8%	[110]
Poly(L-lactic acid) nanofibers	Glucose	1 × 10 <sup>5</sup> to 5 × 10 <sup>6</sup> ng mL <sup>-1</sup>	1 × 10 <sup>5</sup> ng mL <sup>-1</sup>	-	-	[111]
Cobalt (II)-terephthalate MOFs	Glucose	5 × 10 <sup>4</sup> to 1.5 × 10 <sup>7</sup> nmol L <sup>-1</sup>	3.2 × 10 <sup>3</sup> nmol L <sup>-1</sup>	Human blood	96.9% to 102.6%	[112]

ssDNA-PEI-Au-PS: single strand DNA (ssDNA) functionalized polyethyleneimine (PEI) encapsulation of gold-decorated polystyrene (PS) core particles; AgNPs: silver nanoparticles; PVP: poly(vinylpyrrolidone); NCs: nanoclusters; PdNPs: palladium nanoparticles; Pd NPs/meso-C: mesoporous carbon-dispersed PdNPs; PtNPs: platinum nanoparticles; AuNRs: gold nanorods; ZnONRs: zinc oxide nanorods; Ig G: immunoglobulin G; NADH: aihydronicotinamide adenine dinucleotide; H-FABP: heart-type fatty acid-binding protein; sIL-2R: soluble interleukin-2 receptor.

Comparison with natural enzymes, nanomaterials with enzyme-like characteristics (i.e., nanozymes), such as magnetic nanoparticles, noble metal nanoparticles, MOFs, heterojunctions, etc., exhibit several advantages, including easy production with large-scale, low cost and high stability in harsh environments. These unique properties endow them with attractive applications in the fabrication of PADs with high analytical performance [104,111,112]. Zhang et al. developed a ready-to-use PAD for the determination of  $\text{H}_2\text{O}_2$  by simply immobilization of mesoporous carbon-dispersed palladium nanoparticles (Pd NPs/meso-C) and the 3,3',5,5'-tetramethylbenzidine (TMB) substrate onto a common chromatography paper [104]. Taking the advantage of large surface area of the meso-C support and the good dispersity of PdNPs, the PdNPs/meso-C show excellent catalytic performance to trigger the chromogenic reaction of colorless TMB to blue TMB<sub>ox</sub> mediated by  $\text{H}_2\text{O}_2$ . The as-developed PAD exhibited a linear range of 5 to 300  $\text{mol L}^{-1}$ , and can be used to determine  $\text{H}_2\text{O}_2$  in complex matrices, such as milk. Kitchawengkul et al. developed a laminated three-dimensional (3D)- $\mu$ PAD for colorimetric determination of total cholesterol (TC) in human blood by using the peroxidase-like activity of nitrogen-doped CDs (N-CDs) [108]. The 3D- $\mu$ PAD with a 6 mm circular detection zone was fabricated by a simple wax screen-printing technique, which consisted of four layers laminated together vertically. The 3D- $\mu$ PAD exhibited a linear range of 0.05 to 10  $\text{mmol L}^{-1}$  with an LOD of 0.014  $\text{mmol L}^{-1}$ . In particular, TC in human blood could be determined by the naked eye within 10 min by simple comparison with a color chart. Overall, the as-proposed 3D- $\mu$ PAD serves as a simple, low cost, rapid, sensitive and selective alternative for detection of TC in whole blood samples that is friendly to unskilled end users. Cui et al. fabricated an origami PAD (oPAD) assisted by Pd decorated Cu/Co co-doped  $\text{CeO}_2$  (CuCo- $\text{CeO}_2$ -Pd) nanospheres, for dual-mode electrochemical/visual detection of amyloid- $\beta$  ( $\text{A}\beta$ ) peptide with high sensitivity [48]. In this case, the CuCo- $\text{CeO}_2$ -Pd nanospheres were introduced as an enhanced "signal transducer layer", which act as an outstanding catalyst for catalyzing glucose to produce  $\text{H}_2\text{O}_2$  for DPV signal readout and further 3,3',5,5'-tetramethylbenzidine (TMB) oxidation for colorimetric analysis. The oPAD exhibited linear ranges from 1.0  $\text{pmol L}^{-1}$  to 100  $\text{nmol L}^{-1}$  (EC detection) and 10  $\text{pmol L}^{-1}$  to 100  $\text{nmol L}^{-1}$  (visual detection) with LODs of 0.05  $\text{pmol L}^{-1}$  (EC detection) and 0.5  $\text{pmol L}^{-1}$  (visual detection), respectively. The oPAD was used successfully to analysis  $\text{A}\beta$  peptide in artificial cerebrospinal fluid (aCSF) and serum samples. Al Lawati et al. developed a PAD for the colorimetric/fluorometric monitoring of glucose by co-immobilizing two-dimensional cobalt-terephthalate MOF nanosheets (2D CoMOFs) and GOX on chromatography paper [112]. Due to its highly porous and extraordinarily stable structures, the 2D CoMOF increased significantly the stability and performance of GOX, and also acted as a catalyst to accelerate the reaction of  $\text{H}_2\text{O}_2$  produced by the enzymatic oxidation of glucose with o-phenylenediamine (OPD) serving as a peroxidase substrate, resulting in a yellow-brown color change and a high fluorescence emission. The as-developed PAD showed high analytical performance for the quantification of glucose including high accuracy, wide linear range (50  $\text{mol L}^{-1}$  to 15  $\text{mmol L}^{-1}$ ) and low LODs (16.3 (colorimetric detection) and 3.2  $\text{mmol L}^{-1}$  (fluorometric detection)), and was used successfully to determine glucose in blood samples from healthy and diabetic volunteers.

### 2.3. Fluorometric Paper-Based Analytical Devices

Recently, the nanomaterial-based fluorometric PADs are increasingly being developed for sensing various targets (as shown in Table 3) [113–161]. The schematic diagram of the working principle of the fluorometric PAD is shown in Figure 5. The reaction process of the analyte on the test strip is common with that of the colorimetric test strip. After the reaction is finished, the fluorometric signals of emission wavelengths at the test and control zones are recorded by fluorometric spectrophotometer under irradiating with excitation light. Fluorescent nanomaterials, including metal nanoclusters (NCs), CDs, QDs, UCNPs and MOFs, have unique properties, such as wide excitation wavelength, narrow emission band, tunable fluorescence color, highly optical stability and good surface-modified

flexibility. For instance, Ungor et al. developed a fluorescent PAD with red-emitting ( $\lambda_{\text{emission}} = 645 \text{ nm}$ ,  $d = 1.5 \pm 0.3 \text{ nm}$ ) fluorescent gold nanoclusters (AuNCs) for rapid detection of L-kynurenine (Kyn) with an LOD of  $5 \mu\text{mol L}^{-1}$ , which is in good accordance with the toxic Kyn concentration of liquor and serum for several cancers (vulvar, ovarian cancer and leukemia) [116]. Lert-itthiporn et al. reported a fluorescent PAD for membraneless gas-separation with subsequent determination of iodate ( $\text{IO}_3^-$ ) by fabrication of two circular reservoirs (donor reservoir and the acceptor reservoir) in a folded chromatography paper [117]. The  $\text{IO}_3^-$  is reduced to free iodine (I) by iodide ( $\text{I}^-$ ) in the donor reservoir, while the gold core of the bovine serum albumin-stabilized gold NCs (BSA-AuNCs) in the acceptor reservoir is etched by diffused I from the donor reservoir, which results in the quenching of the red emission of BSA-AuNCs in the acceptor reservoir. After folding, the donor reservoir and acceptor reservoir were mounted together through a two-sided mounting tape to allow membraneless gas-separation of free I from the donor reservoir to diffuse into the acceptor reservoir. Under the ultraviolet (UV) light (365 nm) irradiation, the PAD exhibited a linear range from 0.005 to  $0.1 \text{ mmol L}^{-1}$ , an LOD of  $0.01 \text{ mmol L}^{-1}$ , high accuracy (mean recovery:  $95.1 (\pm 4.6) \%$ ) and high precision (RSD < 3%), which was applied successfully for the measurement of  $\text{IO}_3^-$  in iodized salts and fish sauces without prior sample pre-treatment. Yin et al. developed a fluorescent/colorimetric dual-model PAD based on the quenching effect of graphitic carbon nitride on palladium nanoclusters (PdNCs) for detection of miRNA let-7a [119]. In this case, the PdNCs not only was used as a fluorescence probe but also could catalyze a chromogenic reaction for the generation of color change. Combined with nucleic acid cycle signal amplification, the fluorescent/colorimetric dual-model PAD exhibited linear ranges of  $50 \text{ pmol L}^{-1}$  to  $1 \text{ mol L}^{-1}$  (colorimetry) and  $10 \text{ fmol L}^{-1}$  to  $1 \text{ nmol L}^{-1}$  with LODs  $16 \text{ pmol L}^{-1}$  (colorimetry) and  $3 \text{ fmol L}^{-1}$  (fluorescence), respectively. In addition, the fluorescent/colorimetric PAD has excellent stability (about 90% of the fluorescent response remaining after 6 weeks) and good reproducibility (both of intra-assay and inter-assay RSDs were less than 5.5%). The experimental results demonstrate that the fluorescent/colorimetric dual-model PAD can be used for on-site detection of miRNAs with good analytical performance.

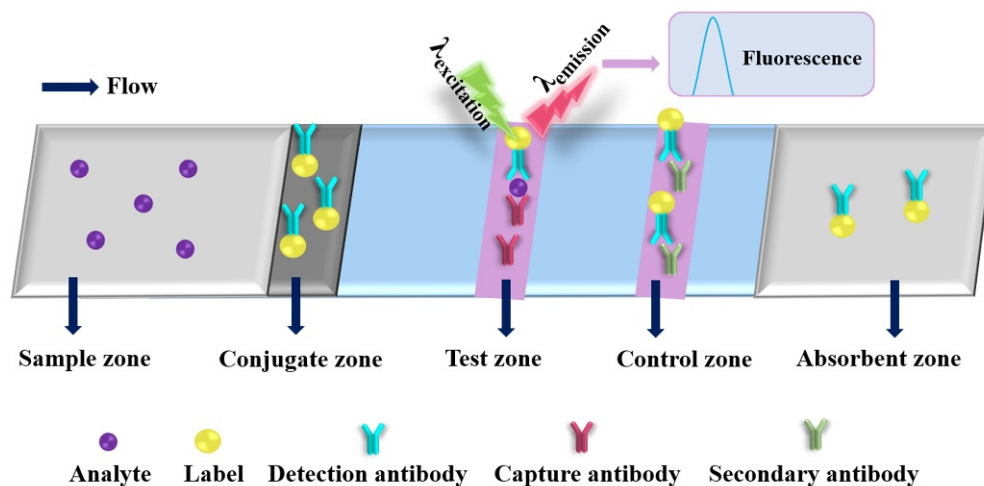


**Figure 5.** Schematic diagram of a typical fluorometric paper-based analytical device.

**Table 3.** The typical nanomaterial-enhanced fluorescent PADs for sensing various analytes.

Nanomaterials	Analytes	Linear Ranges	Limit of Detection	Real Samples	Recovery	Ref.
AuNCs/MIL-68(In)-NH <sub>2</sub> /Cys	Hg <sup>2+</sup>	0.02 nmol L <sup>-1</sup> to 200 nmol L <sup>-1</sup> and 200 to 6 × 10 <sup>4</sup> nmol L <sup>-1</sup>	6.7 × 10 <sup>-3</sup> nmol L <sup>-1</sup>	Tap and Lake water	91.3% to 110.2%	[115]
γG-AuNCs	L-kynurenine (Kyn)	-	5 × 10 <sup>3</sup> nmol L <sup>-1</sup>	Artificial cerebrospinal fluid	-	[116]
BSA-AuNCs	Iodate	5 × 10 <sup>3</sup> to 1 × 10 <sup>5</sup> nmol L <sup>-1</sup>	5 × 10 <sup>3</sup> nmol L <sup>-1</sup>	Iodized salts and fish sauces	90.5% to 102%	[117]
PVP-supported CuNCs	Iodine	100 to 500 ng mL <sup>-1</sup>	29 ng mL <sup>-1</sup>	-	97% to 108%	[118]
Graphitic carbon nitride nanosheets and ssDNA functionalized PdNCs	Let-7a	5 × 10 <sup>-2</sup> to 1 × 10 <sup>3</sup> nmol L <sup>-1</sup> (Colorimetry) and 1 × 10 <sup>-5</sup> to 1 nmol L <sup>-1</sup> (Fluorescence)	1.6 × 10 <sup>-2</sup> nmol L <sup>-1</sup> (Colorimetry) and 3 × 10 <sup>-6</sup> nmol L <sup>-1</sup> (Fluorescence)	Human serum	91% to 110%	[119]
Imprinted polymer grafted CdTe QDs	Cu <sup>2+</sup> , Cd <sup>2+</sup> , Pb <sup>2+</sup> and Hg <sup>2+</sup>	-	10 ng mL <sup>-1</sup> (Cu <sup>2+</sup> ), 7 ng mL <sup>-1</sup> (Cd <sup>2+</sup> ), 9 ng mL <sup>-1</sup> (Pb <sup>2+</sup> ) and 15 ng mL <sup>-1</sup> (Hg <sup>2+</sup> )	Seawater	-	[120]
CdTe QDs	Ag <sup>+</sup> and Ag NPs	50 to 1.1 × 10 <sup>4</sup> ng mL <sup>-1</sup> (Ag <sup>+</sup> )	50 ng mL <sup>-1</sup> (Ag <sup>+</sup> )	River water and antibacterial Products	94% to 115%	[121]
CdTe QDs	2,4-dichlorophenoxyacetic acid	560 to 8 × 10 <sup>4</sup> nmol L <sup>-1</sup>	90 nmol L <sup>-1</sup>	soybean sprouts and lake water	86.2% to 109.5%	[122]
Mercaptosuccinic-acid capped CdTe QDs	Arsenic	50 to 3 × 10 <sup>4</sup> ng mL <sup>-1</sup>	16 ng mL <sup>-1</sup>	Water	92% to 112%	[123]
Silica-embedded CdTe QDs functionalized with rhodamine derivative	Fe <sup>3+</sup>	0 to 3.25 × 10 <sup>3</sup> nmol L <sup>-1</sup>	26.5 nmol L <sup>-1</sup>	Lake water and river water	94.2% to 106.0%	[124]
Polythiophene-coated CdTe QDs	Acetylcholinesterase	-	2.13 U L <sup>-1</sup>	Human serum	107% to 112%	[125]
Antibody functionalized CdTe QD and Au NPs	Immunoglobulin G	10 to 100 ng mL <sup>-1</sup>	0.4 ng mL <sup>-1</sup>	Human serum	97% to 104%	[126]
CdTe QDs and antibody functionalized AgNPs	Matrix metalloproteinase-7 (MMP7)	0.01 to 30 ng mL <sup>-1</sup>	7.3 × 10 <sup>-3</sup> ng mL <sup>-1</sup>	Human serum	91.7% to 113.3%	[127]

Table 3. Cont.

Nanomaterials	Analytes	Linear Ranges	Limit of Detection	Real Samples	Recovery	Ref.
CdTe QDs embedded SiNPs	Alpha fetoprotein (AFP)	0.001 to 20 ng mL <sup>-1</sup>	400 ng mL <sup>-1</sup>	Human serum	-	[130]
CdTe/CdSe QDs	Carcinoembryonic antigen (CEA)	0.05 to 20 ng mL <sup>-1</sup>	6.7 × 10 <sup>-3</sup> ng mL <sup>-1</sup>	Human serum	-	[131]
ZnSe QDs	Cd <sup>2+</sup> and Pb <sup>2+</sup>	1 to 70 ng mL <sup>-1</sup> (Cd <sup>2+</sup> ) and 1 to 60 ng mL <sup>-1</sup> (Pb <sup>2+</sup> )	0.245 ng mL <sup>-1</sup> (Ca <sup>2+</sup> ) and 0.335 ng mL <sup>-1</sup> (Pb <sup>2+</sup> )	Lake water and Seawater	95.0% to 105.1%	[132]
Cd <sub>6</sub> Se <sub>1-x</sub> ZnS (core@shell) QDs	Oligonucleotide biomarkers	-	1.5 × 10 <sup>-3</sup> nmol	-	-	[133]
GNR-QD core-shell embedded MOF structures	Benzaldehyde	2 to 5 × 10 <sup>3</sup> ng mL <sup>-1</sup>	1.2 ng mL <sup>-1</sup>	Human exhalation	-	[134]
ssDNA functionalized QDs coated MSNs and GO	MCF-7, HL-60 and K562 cells	180 to 8 × 10 <sup>7</sup> (MCF-7 cell), 210 to 7 × 10 <sup>7</sup> (HL-60 cell) and 200 to 7 × 10 <sup>7</sup> cells mL <sup>-1</sup> (K562 cell)	62 (MCF-7 cell), 70 (HL-60 cell) and 65 (K562 cell) cells mL <sup>-1</sup>	-	-	[140]
N-CDs	Hg <sup>2+</sup>	1 × 10 <sup>4</sup> to 8 × 10 <sup>5</sup> nmol L <sup>-1</sup>	10.7 nmol L <sup>-1</sup>	-	-	[141]
N-CDs	Hg <sup>2+</sup>	500 to 2.5 × 10 <sup>4</sup> ng mL <sup>-1</sup>	500 ng mL <sup>-1</sup>	Drinking, pond and tap water	80% to 111%	[142]
CDs	Folic acid	1 × 10 <sup>3</sup> to 3 × 10 <sup>5</sup> nmol L <sup>-1</sup>	280 nmol L <sup>-1</sup>	Orange juice and urine	95.8% to 106.2%	[143]
Blue CDs and red CDs	Pb <sup>2+</sup>	0 to 200 nmol L <sup>-1</sup>	2.89 nmol L <sup>-1</sup>	Tap water and lake water	92.8% to 115.2%	[144]
CDs and hexametaphosphate capped AuNPs	Ca <sup>2+</sup> , Mg <sup>2+</sup> and F <sup>-</sup>	0 to 4.5 × 10 <sup>5</sup> nmol L <sup>-1</sup> (F <sup>-</sup> )	2.1 × 10 <sup>4</sup> nmol L <sup>-1</sup> (F <sup>-</sup> )	Ground water	96.2% to 109.5%	[149]
ssDNA functionalized N-CDs and ssDNA functionalized CeO <sub>2</sub> NPs	miRNAs	1 × 10 <sup>-7</sup> to 1 nmol L <sup>-1</sup> (miRNA210) and 2 × 10 <sup>-7</sup> to 2 nmol L <sup>-1</sup> (miRNA21)	3 × 10 <sup>-8</sup> nmol L <sup>-1</sup> (miRNA210) and 6 × 10 <sup>-8</sup> nmol L <sup>-1</sup> (miRNA21)	Cell lysates	96.9% to 103.0%	[151]
CDs@Eu/GMP ICPs	Acetylcholinesterase	0 to 60 mU mL <sup>-1</sup>	2 mU mL <sup>-1</sup>	Brain tissues and cerebrospinal fluid (CSF)	98.3% to 98.8%	[152]

Table 3. Cont.

Nanomaterials	Analytes	Linear Ranges	Limit of Detection	Real Samples	Recovery	Ref.
UCNPs	Immunoglobulin E (IgE)	0.5 to 50 IU mL <sup>-1</sup>	0.13 IU mL <sup>-1</sup>	Human serum	-	[155]
Eu@SiNPs	<i>Bacillus anthrax</i> spores	-	2.38 × 10 <sup>4</sup> spore mL <sup>-1</sup>	Yellow river water, tap water and soil	92.9% to 106.9%	[156]
NH <sub>2</sub> -MIL-125(Ti) MOF and GDH/antibody functionalized AuNPs	CEA	0.1 to 200 ng mL <sup>-1</sup>	0.041 ng mL <sup>-1</sup>	Human serum	-	[157]
Eu-DPA/PTA-NH <sub>2</sub> MOF	H <sub>2</sub> O	0 to 100% v/v	0.01% v/v	Weisu granule, Cefuroxime axetil capsule and Azithromycin capsule	-	[158]
Cu(II)-Pyrazolate-based porphyrinic MOFs	Dopamine	2.5 to 1 × 10 <sup>3</sup> nmol L <sup>-1</sup>	2.5 nmol L <sup>-1</sup>	Human serum	-	[160]
Al-MOF nanosheet	Malachite green	500 to 2 × 10 <sup>5</sup> ng mL <sup>-1</sup>	1.6 × 10 <sup>3</sup> ng mL <sup>-1</sup>	Fish tissue	91.0% to 108.8%	[161]

AuNCs: gold nanoclusters; AuNCs/MIL-68(In)-NH<sub>2</sub>/Cys: glutathione stabilized AuNCs/indium-based MOFs modified with cysteine; BSA-AuNCs: bovine serum albumin-stabilized AuNCs; γG-AuNCs: γ-globulin (γG) immunoprotein stabilized AuNCs; SiNPs: silica nanoparticles; MSNs: mesoporous silica nanoparticles; UCNPs: upconversion nanoparticles; Eu@SiNPs: europium (Eu)-doped silicon nanoparticles; GDH: glutamate dehydrogenase; Eu-DPA/PTA-NH<sub>2</sub> MOF: Eu-dipicolinic acid/2-aminophthalic acid MOF; ICP: ion concentration polarization.

QDs are generally good donors for the fabrication of FRET sensing platforms since the fluorescence of QDs is easily quenched by many substances. Liu et al. reported a fluorescent PAD for detection of  $\text{Ag}^+$  and AgNPs by inkjet-printing CdTe QDs on Whatman® grade 3030–861 chromatography paper because  $\text{Ag}^+$  enables to quench the fluorescence of CdTe QDs via a cation exchange reaction between  $\text{Ag}^+$  and the CdTe QDs [121]. Under optimized conditions, the as-proposed PAD exhibited high analytical performance of  $\text{Ag}^+$  or AgNPs (pretreated by  $\text{HNO}_3$ ), including high selectivity, low LOD ( $0.05 \mu\text{g mL}^{-1}$ ) and good accuracy (4.5% and 2.2% RSDs for  $1 \mu\text{g mL}^{-1}$  and  $7 \mu\text{g mL}^{-1}$  of  $\text{Ag}^+$ , respectively). In addition, the practicality of the fluorescent PAD was demonstrated by detecting  $\text{Ag}^+$  and AgNPs in river water and 12 commercial products, including four textiles, three gynecological lotions, one surgical dressing and four baby products. Zhou et al. developed a 3D rotary fluorescent PAD for multiplexed detection of  $\text{Cd}^{2+}$  and  $\text{Pb}^{2+}$  by transferring the liquid phase of ZnSe QDs@ion imprinted polymers to solid glass fiber paper [132]. Under optimized experiment conditions, the as-proposed 3D rotary fluorescent PAD exhibited a linear range from 1 to  $70 \text{ ng mL}^{-1}$  with an LOD of  $0.245 \text{ ng mL}^{-1}$  for  $\text{Cd}^{2+}$ , and a linear range from 1 to  $60 \text{ ng mL}^{-1}$  with an LOD of  $0.335 \text{ ng mL}^{-1}$  for  $\text{Pb}^{2+}$ , respectively. Qu et al. developed a fluorescent PAD based on polythiophene (CP)-CdTe QD conjugates for detection of acetylcholinesterase (AChE) by turning on the fluorescence of the CP-CdTe QD conjugates via the interaction between CP and thiocholine produced by ATCh hydrolysis and aggregation induced emission enhancement (AIEE) [125]. Under optimized conditions, the as-developed fluorescent PAD exhibited a low LOD of  $0.14 \text{ U L}^{-1}$ . Zhang et al. developed a fluorescent PAD for the ratiometric fluorescence determination of 2,4-dichlorophenoxyacetic acid through fluorescence resonance energy transfer (FRET) of nitrobenzoxadiazole (NBD) and CdTe QDs [122]. Under optimized conditions, the as-developed fluorescent PAD exhibited a linear range of 0.56 to  $80 \mu\text{mol L}^{-1}$  with an LOD of  $90 \text{ nmol L}^{-1}$ . The PAD was applied successfully for detection of 2,4-dichlorophenoxyacetic acid in spiked soybean sprouts and lake water samples with high recovery rates ranging from 86.2% to 109.5% and the RSD less than 4.19%.

As a new class of fluorescent nanomaterials, CDs (also known as carbon QDs and carbon dots) have been used to fabricate fluorescent PADs because of their superior merits, such as easy synthesis, biocompatibility, environmental friendliness, fluorescence tunability and stable luminescent emission [141–152]. Wang et al. developed an instrument-free fluorescent PAD for detection of  $\text{Pb}^{2+}$  by directly inject-printing dual-emission CDs (blue CDs and red CDs) in A4 paper [144]. The blue fluorescence was quenched by  $\text{Pb}^{2+}$ , while the red fluorescence was kept unchanged. The as-developed fluorescent PAD can detect as low as  $2.89 \text{ nmol L}^{-1}$   $\text{Pb}^{2+}$  under a 365 nm UV lamp irradiation. The fluorescent PAD was used successfully to determine  $\text{Pb}^{2+}$  in real samples, including tap water and lake water. Tian et al. developed a fluorescent PAD for detection of  $\text{F}^-$  in water by immobilizing the  $\text{Ca}^{2+}$ , CDs and hexametaphosphate capped AuNPs on the cellulose chromatography paper [149]. Under a 365 nm UV lamp irradiation, the fluorescence color of the PAD changed from orange to blue through the aggregation induced FRET mechanism when various concentrations of  $\text{F}^-$  (0, 100, 200, 300 and  $400 \text{ mol L}^{-1}$ ) were applied. Li et al. developed a fluorescent PAD based on hybrid polydimethylsiloxane (PDMS)/paper for detection of folic acid (FA) by using CDs as fluorophores, which were immobilized on the cellulose paper by Schiff base chemistry [143]. Under optimized conditions, the as-developed fluorescent PAD exhibited a wide range of 1 to  $300 \mu\text{mol L}^{-1}$  with an LOD of  $0.28 \mu\text{mol L}^{-1}$ . The feasibility of the fluorescent PAD was further verified by detection of FA in orange juice and urine samples with satisfactory results. Liang et al. developed a flower-like AgNPs (FLS)-enhanced fluorescent/visual bimodal PAD for detection of multiple miRNAs [151]. In this case, the ssDNA functionalized CDs (DNA1-N-CDs) were immobilized on the FLS layer, which was in situ grown on the surfaces of cellulose fibers of chromatography paper. The fluorescences of DNA1-N-CDs were quenched by ssDNA functionalized  $\text{CeO}_2$  NPs (DNA2- $\text{CeO}_2$ ) through DNA hybridization. In the presence of miRNA, the fluorescent intensities of DNA1-N-CDs were recovered and strengthened by

FLS. The disengaged DNA2-CeO<sub>2</sub> could result in color change after adding H<sub>2</sub>O<sub>2</sub>, leading to the real-time visual detection of miRNA. The as-developed FLS-enhanced fluorescent PAD exhibited linear ranges of 0.1 fmol L<sup>-1</sup> to 1 nmol L<sup>-1</sup> and 0.2 fmol L<sup>-1</sup> to 2 nmol L<sup>-1</sup> for miRNA210 and miRNA21 with LODs of 0.03 fmol L<sup>-1</sup> for miRNA210 and 0.06 fmol L<sup>-1</sup> for miRNA21, respectively. The practicability of the FLS-enhanced fluorescence PAD was demonstrated by successful detection of miRNA210 in different cell lysates.

Because of NIR-excitation and the visible light emission nature of UCNPs, the fluorescent PADs using UCNPs as the label can avoid the interference of autofluorescence and scattering light from biological samples and paper substrates, resulting in an improvement in the detection accuracy of the PAD [153–155]. Recently, He et al. developed a UCNP-based fluorescent PAD for detection of total immunoglobulin E (IgE) in human serum through resonance energy transfer between UCNPs and organic dye tetramethylrhodamine (TAMRA) [155]. The UCNP-based fluorescent PAD exhibited a linear range of 0.5 to 50 IU mL<sup>-1</sup> with an LOD of 0.13 IU mL<sup>-1</sup>. The practicability of the UCNP-based fluorescent PAD was demonstrated by the determination of IgE in 20 human serum samples. The results of the UCNP-based PAD were well consistent with those of the commercial ELISA kit. The RSDs (n = 3) of the PAD varied from 2.7% to 19.7%. The results suggested that the UCNP-based fluorescent PAD could be used as a POCT device for individual diagnostic and real-time detection.

Recently, a MOFs-based fluorescent PAD has been developed for the detection of various targets [157–161]. Lv et al. developed a fluorescent PAD for detection of CEA through wet NH<sub>3</sub>-triggered structural change of NH<sub>2</sub>-MIL-125(Ti) impregnated on paper [157]. The NH<sub>2</sub>-MIL-125(Ti)-based PAD exhibited a linear range of 0.1 ng mL<sup>-1</sup> to 200 ng mL<sup>-1</sup> with an LOD of 0.041 ng mL<sup>-1</sup>. Yue et al. developed a portable smartphone-assisted ratiometric fluorescent PAD for detection of malachite green (MG) by using fluorescent Al-MOF nanosheet and rhodamine B (RhB) as fluorescent probes [161]. The as-developed fluorescent PAD exhibited a wide linear range of 0.5 to 200 µg mL<sup>-1</sup>, a low LOD of 1.6 µg mL<sup>-1</sup>, satisfactory recoveries (in the range of 81.90% to 108.00% and low RSD (in the range of 1.00% to 4.69%). The practicability of the fluorescent PAD was verified by detection of MG in spiked fish tissues. The as-obtained results were in good agreement with those obtained by high performance liquid chromatography (HPLC).

#### 2.4. Paper-Based Surface-Enhanced Raman Spectroscopic Analytical Devices

The basic principle of SERS is that the signal of the analyte is strongly amplified through LSPR phenomena (i.e., electromagnetic hot spots) generated by light when it interacts with labels (plasmonic metal nanoparticles), such as gold nanorods (GNRs) and AgNPs, as shown in Figure 6. The PAD-based SERS substrates have gained considerable attention since they enable on-site label-free detection of a wide variety of analytes and provide “fingerprint” signatures of analytes (as shown in Table 4) [134,162–176]. Saha and Jana developed a PAD-based SERS assay for the detection of proteins by mixing plasmonic nanomaterials (silver coated AuNPs (Ag@AuNPs)) and analyte in the mobile phase, where the analyte induced Ag@Au nanoparticles form controlled aggregates and generate electromagnetic hot spots inside the microfluidic channel, resulting in a strong SERS signal [173]. The as-developed PAD-based SERS assay exhibited high reproducibility and sensitivity, which can be used to detect 1 fmol L<sup>-1</sup> concanavalin A within 3 min. Qi et al. developed an oPAD for miRNA detection through modification of DNA-encoded Raman-active anisotropic AgNPs in the hydrophilic channels [171]. In the presence of analyte, the Raman signals on DNA-encoded AgNPs were amplified through a target-dependent, sequence-specific DNA hybridization assembly. The simple and low-cost oPAD is generic and applicable to various miRNAs, which holds promising applications in point-of-care diagnostics because it can be used to detect as low as 1 pmol L<sup>-1</sup> within 15 min. Wu et al. developed a PAD for detection of acrylamide (AAM) in food products by using the strawberry-like SiO<sub>2</sub>/Ag nanocomposites (SANC) immersed chromatography paper [172]. Under the optimized conditions, the as-developed PAD SERS assay exhibited

a wide linear response from  $0.1 \text{ nmol L}^{-1}$  to  $50 \text{ } \mu\text{mol L}^{-1}$  with a low LOD of  $0.02 \text{ nmol L}^{-1}$  and good recoveries of 80.5% to 105.6% for practical samples, including cookies, chips and bread. In addition, the total assaying time of the PAD was less than 10 min. The result indicated that the PAD SERS assay could be a promising strategy in food analysis and verification. Li et al. developed a colorimetric/SERS dual-mode PAD for sensing  $\text{SO}_2$  by immobilization of 4-mercaptopyridine (Mpy)-modified GNRs-reduced graphene oxide (rGO) hybrids (rGO/MPy-GNRs), anhydrous methanol and starch-iodine complex into cellulose-based chromatography paper through a vacuum filtration method [174]. The PAD can be used not only as a naked-eye indicator of  $\text{SO}_2$  changed from blue to colorless but also as a highly sensitive SERS substrate because of the  $\text{SO}_2$ -triggered conversion of Mpy to pyridine methyl sulfate on the GNRs. The PAD-based SERS method exhibited a wide linear range from  $1 \text{ } \mu\text{mol L}^{-1}$  to  $2000 \text{ } \mu\text{mol L}^{-1}$  with a low LOD of  $1 \text{ } \mu\text{mol L}^{-1}$ . The colorimetric/SERS method was employed for the detection of  $\text{SO}_2$  in wine, and the as-obtained results matched well with those obtained from the traditional Monier-Williams method. In addition, the color intensities and profiles of the SERS spectra of the colorimetric/SERS dual-mode PAD after 10 weeks are very similar to those of freshly prepared PADs, indicating excellent stability of the colorimetric/SERS dual-mode PAD. This study provides a new strategy for designing of paper-based sensing platform for a wide range of on-site testing applications. Moreover, taking advantage of different nanomaterials, Xia et al. developed a smart PAD (named as vapor generation (paper-based thin-film microextraction system) capable of both sensitive on-site fluorescence detection and accurate SERS quantification of volatile benzaldehyde (BA) by utilizing stimuli-responsive core@shell GNR@QD-embedded MOF structures [125]. The fluorescence emission of carboxyl-capped QDs was completely quenched by amino-modified GNRs via electrostatic interaction. In the presence of BA, the GNRs-QD assemblies was dissociated through the Schiff base reactions between the amine group of 4-mercaptonoaniline and the aldehyde moiety of BA, resulting in the increase in the fluorescence and Raman signal of the hybrid systems. In addition, gaseous BA molecules can be efficiently and selectively concentrated on the GNR surface through the “cavity-diffusion” effect of porous MOF shells, allowing the discrimination of BA in exhaled breath rapidly and precisely even at the sub-ng  $\text{mL}^{-1}$  level with excellent specificity against other volatile organic compounds. The as-developed fluorescent/SERS dual-mode PAD was used successfully to accurately discriminate lung cancer from controls.

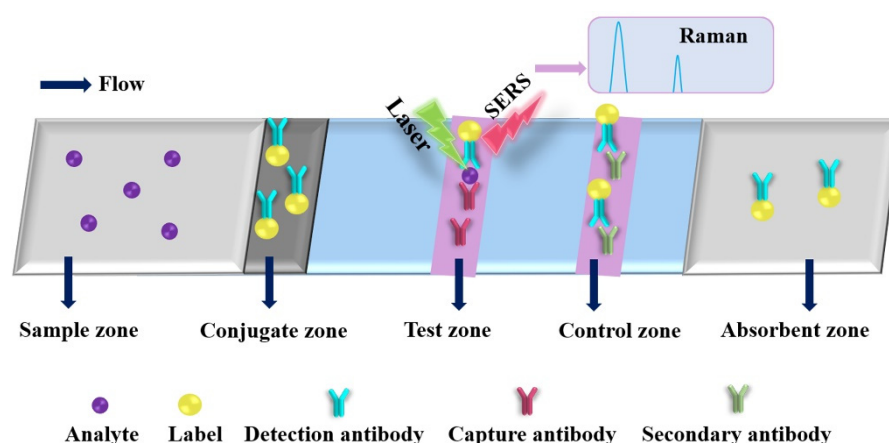


**Figure 6.** Schematic diagram of a typical paper-based surface-enhanced Raman spectroscopic analytical device.

**Table 4.** The typical nanomaterial-based SERS PADs for sensing various analytes.

Nanomaterials	Analytes	Linear Ranges	Limit of Detection	Real Samples	Recovery	Ref
GNR-QD core–shell embedded MOF structures	Benzaldehyde	0.1 to 10 ng mL <sup>-1</sup>	0.1 ng mL <sup>-1</sup>	Human exhalation	-	[134]
GNRs	Fluorescein and naphthalenethiol	-	~1 × 10 <sup>-7</sup> nmol L <sup>-1</sup> (Fluorescein) and 5 × 10 <sup>-10</sup> nmol L <sup>-1</sup> (Naphthalenethiol)	Tap water	-	[162]
GNRs modified with 4-mercaptophenylboronic acid (4-MBA) and 1-decanethiol (1-DT) molecules	Glucose	5 × 10 <sup>5</sup> to 1 × 10 <sup>7</sup> nmol L <sup>-1</sup>	1 × 10 <sup>5</sup> nmol L <sup>-1</sup>	Blood	88%	[163]
AuNPs	Cocaine	-	10 ng mL <sup>-1</sup>	Human plasma	-	[164]
AuNPs	Age-related macular degeneration aqueous humors: THV-I <sub>1043</sub> , THV-I <sub>1454</sub> and THV-I <sub>1656</sub>	-	-	Aqueous humors	-	[165]
AuNPs	Clenbuterol	1 × 10 <sup>-4</sup> to 1 × 10 <sup>2</sup> ng mL <sup>-1</sup>	1 × 10 <sup>-4</sup> ng mL <sup>-1</sup>	Swine hair	104.8% to 116.2%	[166]
AgNPs	P-selectin	100 to 500 ng mL <sup>-1</sup>	104.2 ng mL <sup>-1</sup> (ca. 0.7 nmol L <sup>-1</sup> )	-	-	[167]
Flower-like AgNPs	Chloramphenicol	1 × 10 <sup>-2</sup> to 1 × 10 <sup>5</sup> ng mL <sup>-1</sup>	1 × 10 <sup>-2</sup> ng mL <sup>-1</sup>	Pork	90% to 102%	[168]
Silver nanocubes	Adenine	10 to 1 × 10 <sup>5</sup> nmol L <sup>-1</sup>	0.89 nmol L <sup>-1</sup>	Urine	89% to 107%	[169]
4-aminothiophenol-modified rGO/ Ag NPs	Formaldehyde (FA) and acetaldehyde (AA)	4.5 × 10 <sup>-4</sup> to 480 ng mL <sup>-1</sup>	1.5 × 10 <sup>-4</sup> ng mL <sup>-1</sup> (FA) and 1.3 × 10 <sup>-3</sup> ng mL <sup>-1</sup> (AA)	Wine and human urine	104.6% to 112.8%	[170]
ssDNA functionalized anisotropic AgNPs	Has-miR-21	-	1 pmol L <sup>-1</sup>	-	-	[171]
Strawberry-like SiO <sub>2</sub> / Ag nanocomposites	Acrylamide	0.1 to 5 × 10 <sup>4</sup> nmol L <sup>-1</sup>	0.02 nmol L <sup>-1</sup>	Cookies, chips and bread	80.5% to 105.6%	[172]
Silver coated AuNPs functionalized with 4-Mercapto Pyridine and glucose or 4-mercapto pyridine and biotin.	Streptavidin and concanavalin A	-	1 × 10 <sup>-5</sup> nmol L <sup>-1</sup> (Streptavidin) and 1 × 10 <sup>-6</sup> nmol L <sup>-1</sup> (Concanavalin A)	-	-	[173]
4-mercaptopyridine (Mpy)-modified GNRs-rGO hybrids	SO <sub>2</sub>	1 × 10 <sup>3</sup> to 2 × 10 <sup>6</sup> nmol L <sup>-1</sup>	1 × 10 <sup>3</sup> nmol L <sup>-1</sup>	Wine	87.1% to 116.8%	[174]
ZnO NPs	SO <sub>2</sub>	5 × 10 <sup>3</sup> to 3 × 10 <sup>5</sup> ng mL <sup>-1</sup>	2 × 10 <sup>3</sup> ng mL <sup>-1</sup>	Wine	-	[175]
MoO <sub>3-x</sub> nanosheets	Rhodamine 6G	-	100 nmol L <sup>-1</sup>	-	-	[176]

### 2.5. Comparison of the Detection Methods of Paper-Based Analytical Devices

The above introduced detection methods of PADs indicate that their detection performances have been greatly enhanced with the great advance of nanofabrication science. For the convenience of the readers, the merits and drawbacks of the four major PAD detection methods (EC, colorimetric, fluorometric, SERS PADs) are compared and summarized in Table 5.

**Table 5.** The comparison of four representative detection methods of PADs.

Detection Methods	The Main Nanomaterials	Advantages	Disadvantages	Limit of Detection	Ref.
EC PADs	AuNPs, graphene, MOF, multiple metallic NPs composites and functionalized NPs	High sensitivity, rapid response and easy miniaturization	Equipment-dependent, complicated operation, easy interfered with complex matrices	1 pg mL <sup>-1</sup> level for AuNPs, 0.1 pg mL <sup>-1</sup> level for graphene, 0.1 mmol L <sup>-1</sup> level for MOF, 1 × 10 <sup>-3</sup> pg mL <sup>-1</sup> level for multiple metallic NPs composites and 1 × 10 <sup>-2</sup> pg mL <sup>-1</sup> level for functionalized NPs	[40,50,56,68,75]
Colorimetric PADs	Functionalized AuNPs and AgNPs, enzyme-like nanomaterials	Simplicity and convenience, readout with naked eye, rapidness, low cost and low sample consumption	Poor sensitivity, limited to qualitative or semi-quantitative analysis	10 pg mL <sup>-1</sup> level for functionalized AuNPs, 100 pmol L <sup>-1</sup> level for functionalized AgNPs, 1 pmol L <sup>-1</sup> level for enzyme-like nanomaterials	[48,89,95]
Fluorometric PADs	NC, QD, CD, MOF	Low cost, easy operation	Reader-dependent	1 pmol L <sup>-1</sup> level for NC, 1 pg mL <sup>-1</sup> level for QD, 1 × 10 <sup>3</sup> pg mL <sup>-1</sup> level for CD, 10 pg mL <sup>-1</sup> level for MOF	[115,127,144,157]
SERS PADs	AuNPs and AgNPs	On-site label-free detection, offered fingerprint signatures, high sensitivity	Equipment-dependent	1 pg mL <sup>-1</sup> level for AuNPs and AgNPs	[166,170]

### 3. Conclusions and Perspective

The PADs have gained remarkable consideration as simple, low-cost and powerful POCT platforms since the first commercialized lateral flow immunoassay (LFIA) was used for a home pregnancy test. Although PADs have achieved great success in the rapid testing area, some parameters on the analytical performance of PADs need to be further improved to meet the specific needs of different detection fields. Integrating nanomaterials/nanotechnology into PADs can help improve their analytical performance, including sensitivity, selectivity, reproducibility, stability and multiplexed analysis. For instance, the sensitivity of ePADs can be increased significantly when carbon nanomaterials with high conductivity and high specific surface area are used as electrode materials or electrode modifiers. The AuNPs are commonly used color indicators of colorimetric PADs. The sensitivity of colorimetric PADs will be further increased when AuNPs are conjugated with other catalytic NPs, such as CeO<sub>2</sub> NPs, and/or enlarged through the metallic atoms (such as Au or Ag) surface deposition strategy. In comparison with organic dyes, the fluorescent nanomaterials, including QDs, CDs and metallic NCs, have wide excitation wavelength, high fluorescence brightness and strong resistance to photobleaching, resulting in the excellent stability, reliability and accuracy of PADs. Because the upconverted phosphorescence of UCNP can efficiently avoid the interference of biological autofluorescence, the reliability and accuracy of PADs can also be improved by using UCNP as a fluorescence probe. Nanozymes such as CeO<sub>2</sub> NPs and MOFs have higher robustness than natural enzymes. Therefore, the PADs exhibit high stability and sensitivity, while the nanozymes are used for signal amplification in the PAD fabrication. Meanwhile, the nanomaterials have surface-functionalized flexibility for creating multiple reactive/recognizable sites with analytes to achieve multiplexed analysis. In addition, the nanomaterial-based PADs

are compatible with dual-mode detection, such as colorimetry–fluorescence and EC-optical detection, which enables the reliability and accuracy of the PADs.

The nanomaterial-based PADs have managed great achievements for sensing various targets, including ions, small molecules, nucleic acids, proteins and pathogens, in the bench research. However, there are limited examples that have transformed from proof-of-principle analytical devices to commercial products. More efforts should be made continuously to develop novel strategies for increasing the longevity, robustness and reliability in the real-time monitoring, which are largely dependent on the synthesis of advanced nanomaterials, introduction of a new sensing mechanism and multiple detection modes, development of a reliable microfabricating methodology/standard and simplifying the detection procedures. The next generation of PADs will be simple, cost-effective and multiplexed and be able to provide on-site qualitative/quantitative analysis by the naked eye and/or portable equipment, such as smartphones and wearable electronic devices.

**Author Contributions:** Writing—original draft preparation, R.P., Q.Z., X.M. and Z.W.; writing review and editing, R.P., Q.Z., J.W., X.M. and Z.W. All authors have read and agreed to the published version of the manuscript.

**Funding:** This work was supported by the National Natural Science Foundation of China (Grant No. 21775145), and Science and Technology Developing Foundation of Jilin Province (Grant No. 20210204049YY) for financial support.

**Institutional Review Board Statement:** Not applicable.

**Informed Consent Statement:** Not applicable.

**Data Availability Statement:** Not applicable.

**Acknowledgments:** The authors would like to thank the National Natural Science Foundation of China and Science and Technology Developing Foundation of Jilin Province for financial support.

**Conflicts of Interest:** The authors declare no conflict of interest.

## References

1. Cate, D.M.; Adkins, J.A.; Mettakoonpitak, J.; Henry, C.S. Recent Developments in Paper-Based Microfluidic Devices. *Anal. Chem.* **2015**, *87*, 19–41. [[CrossRef](#)]
2. Xia, Y.; Si, J.; Li, Z. Fabrication Techniques for Microfluidic Paper-Based Analytical Devices and Their Applications for Biological Testing: A Review. *Biosens. Bioelectron.* **2016**, *77*, 774–789. [[CrossRef](#)]
3. Ahmed, S.; Bui, M.N.; Abbas, A. Paper-Based Chemical and Biological Sensors: Engineering Aspects. *Biosens. Bioelectron.* **2016**, *77*, 249–263. [[CrossRef](#)]
4. Liu, S.; Su, W.; Ding, X. A Review on Microfluidic Paper-Based Analytical Devices for Glucose Detection. *Sensors* **2016**, *16*, 2086. [[CrossRef](#)]
5. Mahato, K.; Srivastava, A.; Chandra, P. Paper Based Diagnostics for Personalized Health Care: Emerging Technologies and Commercial Aspects. *Biosens. Bioelectron.* **2017**, *96*, 246–259. [[CrossRef](#)]
6. Wang, P.; Kricka, L.J. Current and Emerging Trends in Point-of-Care Technology and Strategies for Clinical Validation and Implementation. *Clin. Chem.* **2018**, *64*, 1439–1452. [[CrossRef](#)]
7. Li, Y.; Feng, L. Progress in Paper-Based Colorimetric Sensor Array. *Chin. J. Anal. Chem.* **2020**, *48*, 1448–1457. [[CrossRef](#)]
8. Lin, Y.; Gritsenko, D.; Feng, S.; Teh, Y.C.; Lu, X.; Xu, J. Detection of Heavy Metal by Paper-Based Microfluidics. *Biosens. Bioelectron.* **2016**, *83*, 256–266. [[CrossRef](#)]
9. Meredith, N.A.; Quinn, C.; Cate, D.M.; Reilly, T.H.; Volckens, J.; Henry, C.S. Paper-Based Analytical Devices for Environmental Analysis. *Analyst* **2016**, *141*, 1874–1887. [[CrossRef](#)]
10. Kaushik, A.; Tiwari, S.; Jayant, R.D.; Marty, A.; Nair, M. Towards Detection and Diagnosis of Ebola Virus Disease at Point-of-Care. *Biosens. Bioelectron.* **2016**, *75*, 254–272. [[CrossRef](#)] [[PubMed](#)]
11. Sriram, G.; Bhat, M.P.; Patil, P.; Uthappa, U.T.; Jung, H.-Y.; Altalhi, T.; Kumeria, T.; Aminabhavi, T.M.; Pai, R.K.; Kurkuri, M.D. Paper-Based Microfluidic Analytical Devices for Colorimetric Detection of Toxic Ions: A Review. *Trends Anal. Chem.* **2017**, *93*, 212–227. [[CrossRef](#)]
12. Altundemir, S.; Uguz, A.K.; Ulgen, K. A Review on Wax Printed Microfluidic Paper-Based Devices for International Health. *Biomicrofluidics* **2017**, *11*, 041501. [[CrossRef](#)]
13. Campbell, J.M.; Balhoff, J.B.; Landwehr, G.M.; Rahman, S.M.; Vaithyanathan, M.; Melvin, A.T. Microfluidic and Paper-Based Devices for Disease Detection and Diagnostic Research. *Int. J. Mol. Sci.* **2018**, *19*, 2731. [[CrossRef](#)] [[PubMed](#)]

14. Hua, M.Z.; Li, S.; Wang, S.; Lu, X. Detecting Chemical Hazards in Foods Using Microfluidic Paper-Based Analytical Devices ( $\mu$ PADs): The Real-World Application. *Micromachines* **2018**, *9*, 32. [[CrossRef](#)] [[PubMed](#)]
15. Wu, M.; Lai, Q.; Ju, Q.; Li, L.; Yu, H.-D.; Huang, W. Paper-Based Fluorogenic Devices for in Vitro Diagnostics. *Biosens. Bioelectron.* **2018**, *102*, 256–266. [[CrossRef](#)] [[PubMed](#)]
16. Restaino, S.M.; White, I.M. A Critical Review of Flexible and Porous SERS Sensors for Analytical Chemistry at the Point-of-Sample. *Anal. Chim. Acta* **2019**, *1060*, 17–29. [[CrossRef](#)]
17. Ming, T.; Luo, J.P.; Liu, J.T.; Sun, S.; Xing, Y.; Wang, H.; Xiao, G.H.; Deng, Y.; Cheng, Y.; Yang, Z.G.; et al. Paper-Based Microfluidic Aptasensors. *Biosens. Bioelectron.* **2020**, *170*, 112649. [[CrossRef](#)]
18. Ding, R.Y.; Cheong, Y.H.; Ahamed, A.; Lisak, G. Heavy Metals Detection with Paper-Based Electrochemical Sensors. *Anal. Chem.* **2021**, *93*, 1880–1888. [[CrossRef](#)]
19. Alahmad, W.; Sahragard, A.; Varanusupakul, P. Online and Offline Preconcentration Techniques on Paper-Based Analytical Devices for Ultrasensitive Chemical and Biochemical Analysis: A Review. *Biosens. Bioelectron.* **2021**, *194*, 113574. [[CrossRef](#)]
20. Ozer, T.; Henry, C.S. Paper-Based Analytical Devices for Virus Detection: Recent Strategies for Current and Future Pandemics. *Trends Anal. Chem.* **2021**, *144*, 116424. [[CrossRef](#)]
21. Fu, L.-M.; Wang, Y.-N. Detection Methods and Applications of Microfluidic Paper-Based Analytical Devices. *Trends Anal. Chem.* **2018**, *107*, 196–211. [[CrossRef](#)]
22. Morbioli, G.G.; Mazzu-Nascimento, T.; Stockton, A.M.; Carrilho, E. Technical Aspects and Challenges of Colorimetric Detection with Microfluidic Paper-Based Analytical Devices (mPADs)—A Review. *Anal. Chim. Acta* **2017**, *970*, 1–22. [[CrossRef](#)]
23. Chinnadayala, S.R.; Park, J.; Ngoc Le, H.T.; Santhosh, M.; Kadam, A.N.; Cho, S. Recent Advances in Microfluidic Paper-Based Electrochemiluminescence Analytical Devices for Point-of-Care Testing Applications. *Biosens. Bioelectron.* **2019**, *126*, 68–81. [[CrossRef](#)]
24. Solhi, E.; Hasanzadeh, M.; Babaie, P. Electrochemical Paper-Based Analytical Devices (ePADs) toward Biosensing: Recent Advances and Challenges in Bioanalysis. *Anal. Methods* **2020**, *12*, 1398–1414. [[CrossRef](#)]
25. Chung, T.H.; Dhar, B.R. Paper-Based Platforms for Microbial Electrochemical Cell-Based Biosensors: A Review. *Biosens. Bioelectron.* **2021**, *192*, 113485. [[CrossRef](#)]
26. Quesada-González, D.; Merkoçi, A. Nanoparticle-Based Lateral Flow Biosensors. *Biosens. Bioelectron.* **2015**, *73*, 47–63. [[CrossRef](#)]
27. Devi, R.V.; Doble, M.; Verma, R.S. Nanomaterials for Early Detection of Cancer Biomarker with Special Emphasis on Gold Nanoparticles in Immunoassays/Sensors. *Biosens. Bioelectron.* **2015**, *68*, 688–698. [[CrossRef](#)]
28. Arduini, F.; Micheli, L.; Moscone, D.; Palleschi, G.; Piermarini, S.; Ricci, F.; Volpe, G. Electrochemical Biosensors based on Nanomodified Screen-Printed Electrodes: Recent Applications in Clinical Analysis. *Trends Anal. Chem.* **2016**, *79*, 114–126. [[CrossRef](#)]
29. Xu, Y.; Liu, M.; Kong, N.; Liu, J. Lab-on-Paper Micro- and Nano-Analytical Devices: Fabrication, Modification, Detection and Emerging Applications. *Microchim. Acta* **2016**, *183*, 1521–1542. [[CrossRef](#)]
30. Ge, S.; Zhang, L.; Zhang, Y.; Lan, F.; Yan, M.; Yu, J. Nanomaterials-Modified Cellulose Paper as a Platform for Biosensing Applications. *Nanoscale* **2017**, *9*, 4366–4382. [[CrossRef](#)] [[PubMed](#)]
31. Wongkaew, N.; Simsek, M.; Griesche, C.; Baeumner, A.J. Functional Nanomaterials and Nanostructures Enhancing Electrochemical Biosensors and Lab-on-a-Chip Performances: Recent Progress, Applications, and Future Perspective. *Chem. Rev.* **2019**, *119*, 120–194. [[CrossRef](#)]
32. Selvakumar, B.; Kathiravan, A. Sensory Materials for Microfluidic Paper Based Analytical Devices—A Review. *Talanta* **2021**, *235*, 122733. [[CrossRef](#)]
33. Patel, S.; Jamunkar, R.; Monisha, D.S.; Patle, T.K.; Kant, T.; Dewangan, K.; Shrivastava, K. Recent Development in Nanomaterials Fabricated Paper-Based Colorimetric and Fluorescent Sensors: A Review. *Trends Environ. Anal. Chem.* **2021**, *31*, e00136. [[CrossRef](#)]
34. Shirshahi, V.; Liu, G. Enhancing the Analytical Performance of Paper Lateral Flow Assays: From Chemistry to Engineering. *Trends Anal. Chem.* **2021**, *136*, 116200. [[CrossRef](#)]
35. Díaz-González, M.; Escosura-Muñiz, A. Strip Modification and Alternative Architectures for Signal Amplification in Nanoparticle-Based Lateral Flow Assays. *Anal. Bioanal. Chem.* **2021**, *413*, 4111–4117. [[CrossRef](#)] [[PubMed](#)]
36. Wang, C.; Liu, M.; Wang, Z.; Li, S.; Deng, Y.; He, N. Point-of-Care Diagnostics for Infectious Diseases: From Methods to Devices. *Nano Today* **2021**, *37*, 101092. [[CrossRef](#)]
37. Hawkes, R.; Niday, E.; Gordon, J. A Dot-Immunobinding Assay for Monoclonal and Other Antibodies. *Anal. Biochem.* **1982**, *119*, 142–147. [[CrossRef](#)]
38. Dungchai, W.; Chailapakul, O.; Henry, C.S. Electrochemical Detection for Paper-Based Microfluidics. *Anal. Chem.* **2009**, *81*, 5821–5826. [[CrossRef](#)] [[PubMed](#)]
39. Baharfar, M.; Rahbar, M.; Tajik, M.; Liu, G.Z. Engineering Strategies for Enhancing the Performance of Electrochemical Paper-Based Analytical Devices. *Biosens. Bioelectron.* **2020**, *167*, 112506. [[CrossRef](#)]
40. Zheng, X.; Li, L.; Cui, K.; Zhang, Y.; Zhang, L.; Ge, S.; Yu, J. Ultrasensitive Enzyme-Free Biosensor by Coupling Cyclodextrin Functionalized Au Nanoparticles and High-Performance Au-Paper Electrode. *ACS Appl. Mater. Interfaces* **2018**, *10*, 3333–3340. [[CrossRef](#)]

41. Pinyorosphathum, C.; Chaiyo, S.; Sae-ung, P.; Hoven, V.; Damsongsang, P.; Siangproh, W.; Chailapakul, O. Disposable Paper-Based Electrochemical Sensor using Thiol-Terminated Poly(2-Methacryloyloxyethyl Phosphorylcholine) for the Label-Free Detection of C-Reactive Protein. *Microchim. Acta* **2019**, *186*, 472. [[CrossRef](#)]
42. Tian, T.; Liu, H.; Li, L.; Yu, J.; Ge, S.; Song, X.; Yan, M. Paper-Based Biosensor for Noninvasive Detection of Epidermal Growth Factor Receptor Mutations in Non-Small Cell Lung Cancer Patients. *Sens. Actuators B Chem.* **2017**, *251*, 440–445. [[CrossRef](#)]
43. Cinti, S.; Cinotti, G.; Parolo, C.; Nguyen, E.P.; Caratelli, V.; Moscone, D.; Arduini, F.; Merckoci, A. Experimental Comparison in Sensing Breast Cancer Mutations by Signal ON and Signal OFF Paper-Based Electroanalytical Strips. *Anal. Chem.* **2020**, *92*, 1674–1679. [[CrossRef](#)]
44. Eksin, E.; Torul, H.; Yarali, E.; Tamer, U.; Papakonstantinou, P.; Erdem, A. Paper-Based Electrode Assemble for Impedimetric Detection of miRNA. *Talanta* **2021**, *225*, 122043. [[CrossRef](#)]
45. Ortone, V.; Matino, L.; Santoro, F.; Cinti, S. Merging Office/Filter Paper-Based Tools for Pre-Concentrating and Detecting Heavy Metals in Drinking Water. *Chem. Commun.* **2021**, *57*, 7100–7103. [[CrossRef](#)] [[PubMed](#)]
46. Benson, J.; Fung, C.M.; Lloyd, J.S.; Deganello, D.; Smith, N.A.; Teng, K.S. Direct Patterning of Gold Nanoparticles using Flexographic Printing for Biosensing Applications. *Nanoscale Res. Lett.* **2015**, *10*, 127. [[CrossRef](#)] [[PubMed](#)]
47. Pavithra, M.; Muruganand, S.; Parthiban, C. Development of Novel Paper Based Electrochemical Immunosensor with Self-Made Gold Nanoparticle Ink and Quinone Derivate for Highly Sensitive Carcinoembryonic Antigen. *Sens. Actuators B Chem.* **2018**, *257*, 496–503. [[CrossRef](#)]
48. Cui, K.; Zhou, C.; Zhang, B.; Zhang, L.; Liu, Y.; Hao, S.; Tang, X.; Huang, Y.; Yu, J. Enhanced Catalytic Activity Induced by the Nanostructuring Effect in Pd Decoration onto Doped Ceria Enabling an Origami Paper Analytical Device for High Performance of Amyloid- $\beta$  Bioassay. *ACS Appl. Mater. Interfaces* **2021**, *13*, 33937–33947. [[CrossRef](#)]
49. Li, L.; Wang, T.; Zhang, Y.; Xu, C.; Zhang, L.; Cheng, X.; Liu, H.; Chen, X.; Yu, J. Editable TiO<sub>2</sub> Nanomaterial-Modified Paper in Situ for Highly Efficient Detection of Carcinoembryonic Antigen by Photoelectrochemical Method. *ACS Appl. Mater. Interfaces* **2018**, *10*, 14594–14601. [[CrossRef](#)]
50. Xue, J.; Zhang, L.; Gao, C.; Zhu, P.; Yu, J. Microfluidic Paper-Based Photoelectrochemical Sensing Platform with Electron-Transfer Tunneling Distance Regulation Strategy for Thrombin Detection. *Biosens. Bioelectron.* **2019**, *133*, 1–7. [[CrossRef](#)]
51. De França, C.C.L.; Meneses, D.; Silva, A.C.A.; Dantas, N.O.; De Abreu, F.C.; Petroni, J.M.; Lucca, B.G. Development of Novel Paper-Based Electrochemical Device Modified with CdSe/CdS Magic-Sized Quantum Dots and Application for the Sensing of Dopamine. *Electrochim. Acta* **2021**, *367*, 137486. [[CrossRef](#)]
52. Mohan, J.M.; Amreen, K.; Kulkarni, M.B.; Javed, A.; Dubey, S.K.; Goel, S. Optimized Ink Jetted Paper Device for Electroanalytical Detection of Picric Acid. *Colloid. Surface. B.* **2021**, *208*, 112056. [[CrossRef](#)]
53. Amatongchai, M.; Sitanurak, J.; Sroysee, W.; Sodanant, S.; Chairam, S.; Jarujamrus, P.; Nacapricha, D.; Lieberzeit, P.A. Highly Sensitive and Selective Electrochemical Paper-Based Device using a Graphite Screen-Printed Electrode Modified with Molecularly Imprinted Polymers Coated Fe<sub>3</sub>O<sub>4</sub>@Au@SiO<sub>2</sub> for Serotonin Determination. *Anal. Chim. Acta* **2019**, *1077*, 255–265. [[CrossRef](#)]
54. Zhang, X.; Bao, N.; Luo, X.; Ding, S. Patchy Gold Coated Fe<sub>3</sub>O<sub>4</sub> Nanospheres with Enhanced Catalytic Activity Applied for Paper-Based Bipolar Electrode-Electrochemiluminescence Aptasensors. *Biosens. Bioelectron.* **2018**, *114*, 44–51. [[CrossRef](#)] [[PubMed](#)]
55. Huang, Y.Z.; Li, L.; Zhang, Y.; Zhang, L.N.; Ge, S.G.; Yu, J.H. Auto-Cleaning Paper-Based Electrochemiluminescence Biosensor Coupled with Binary Catalysis of Cubic Cu<sub>2</sub>O-Au and Polyethyleneimine for Quantification of Ni<sup>2+</sup> and Hg<sup>2+</sup>. *Biosens. Bioelectron.* **2019**, *126*, 339–345. [[CrossRef](#)] [[PubMed](#)]
56. Huang, Y.; Zhang, L.; Zhang, S.; Zhao, P.; Ge, S.; Yu, J. Paper-Based Electrochemiluminescence Determination of Streptavidin Using Reticular DNA-Functionalized PtCu Nanoframes and Analyte-Triggered DNA Walker. *Microchim. Acta* **2020**, *187*, 530. [[CrossRef](#)] [[PubMed](#)]
57. Pokpas, K.; Jahed, N.; McDonald, E.; Bezuidenhout, P.; Smith, S.; Land, K.; Iwuoha, E. Graphene-AuNP Enhanced Inkjet-Printed Silver Nanoparticle Paper Electrodes for the Detection of Nickel(II)-Dimethylglyoxime [Ni(dmgH<sub>2</sub>)] Complexes by Adsorptive Cathodic Stripping Voltammetry (AdCSV). *Electroanalysis* **2020**, *32*, 3017–3031. [[CrossRef](#)]
58. Valentine, C.J.; Takagishi, K.; Umez, S.; Daly, R.; De Volder, M. Paper-Based Electrochemical Sensors using Paper as a Scaffold to Create Porous Carbon Nanotube Electrodes. *ACS Appl. Mater. Interfaces* **2020**, *12*, 30680–30685. [[CrossRef](#)]
59. Tran, V.; Ko, E.; Geng, Y.; Kim, M.; Jin, G.; Son, S.; Hur, W.; Seong, G. Micro-Patterning of Single-Walled Carbon Nanotubes and Its Surface Modification with Gold Nanoparticles for Electrochemical Paper-Based Non-Enzymatic Glucose Sensor. *J. Electroanal. Chem.* **2018**, *826*, 29–37. [[CrossRef](#)]
60. Jampasa, S.; Pummooe, J.; Siangproh, W.; Khongchareonporn, N.; Ngamrojanavanich, N.; Chailapakul, O.; Chaiyo, S. “Signal-On” Electrochemical Biosensor based on a Competitive Immunoassay Format for the Sensitive Determination of Oxytetracycline. *Sens. Actuators B Chem.* **2020**, *320*, 128389. [[CrossRef](#)]
61. Srisomwat, C.; Teengam, P.; Chuaypen, N.; Tangkijvanich, P.; Vilaivan, T.; Chailapakul, O. Pop-up Paper Electrochemical Device for Label-Free Hepatitis B Virus DNA Detection. *Sens. Actuators B Chem.* **2020**, *316*, 128077. [[CrossRef](#)]
62. Pungjunun, K.; Yakoh, A.; Chaiyo, S.; Praphairaksit, N.; Siangproh, W.; Kalcher, K.; Chailapakul, O. Laser Engraved Microapillary Pump Paper-Based Microfluidic Device for Colorimetric and Electrochemical Detection of Salivary Thiocyanate. *Microchim. Acta* **2021**, *188*, 140. [[CrossRef](#)] [[PubMed](#)]
63. Wang, P.; Cheng, Z.; Chen, Q.; Qu, L.; Miao, X.; Feng, Q. Construction of a Paper-Based Electrochemical Biosensing Platform for Rapid and Accurate Detection of Adenosine Triphosphate (ATP). *Sens. Actuators B Chem.* **2018**, *256*, 931–937. [[CrossRef](#)]

64. Pungjunun, K.; Chaiyo, S.; Praphairaksit, N.; Siangproh, W.; Ortner, A.; Kalcher, K.; Chailapaku, O.; Mehmeti, E. Electrochemical Detection of NO<sub>x</sub> Gas Based on Disposable Paper-Based Analytical Device using a Copper Nanoparticles-Modified Screen-Printed Graphene Electrode. *Biosens. Bioelectron.* **2019**, *143*, 111606. [CrossRef]
65. Prasad, K.; Cao, X.; Gao, N.; Jin, Q.; Sanjay, S.; Henaio-Pabon, G.; Li, X. A Low-Cost Nanomaterial-Based Electrochemical Immunosensor on Paper for High-Sensitivity Early Detection of Pancreatic Cancer. *Sens. Actuators B Chem.* **2020**, *305*, 127516. [CrossRef] [PubMed]
66. Wang, Y.; Xu, H.; Luo, J.; Liu, J.; Wang, L.; Fan, Y.; Yan, S.; Yang, Y.; Cai, X. A Novel Label-Free Microfluidic Paper-Based Immunosensor for Highly Sensitive Electrochemical Detection of Carcinoembryonic Antigen. *Biosens. Bioelectron.* **2016**, *83*, 319–326. [CrossRef]
67. Wang, Y.; Luo, J.; Liu, J.; Sun, S.; Xiong, Y.; Ma, Y.; Yan, S.; Yang, Y.; Yin, H.; Cai, X. Label-Free Microfluidic Paper-Based Electrochemical Aptasensor for Ultrasensitive and Simultaneous Multiplexed Detection of Cancer Biomarkers. *Biosens. Bioelectron.* **2019**, *136*, 84–90. [CrossRef]
68. Ortega, F.; Regiart, M.; Rodríguez-Martínez, A.; Miguel-Pérez, D.; Serrano, M.; Lorente, J.; Tortella, G.; Rubilar, O.; Sapag, K.; Bertotti, M.; et al. Sandwich-Type Electrochemical Paper-Based Immunosensor for Claudin 7 and CD81 Dual Determination on Extracellular Vesicles from Breast Cancer Patients. *Anal. Chem.* **2021**, *93*, 1143–1153. [CrossRef]
69. Scala-Benuzzi, M.L.; Raba, J.; Soler-Illia, G.J.A.A.; Schneider, R.J.; Messina, G.A. Novel Electrochemical Paper-Based Immuno-capture Assay for the Quantitative Determination of Ethinylestradiol in Water Samples. *Anal. Chem.* **2018**, *90*, 4104–4111. [CrossRef]
70. Cincotto, F.H.; Fava, E.L.; Moraes, F.C.; Fatibello-Filho, O.; Faria, R.C. A New Disposable Microfluidic Electrochemical Paper-Based Device for the Simultaneous Determination of Clinical Biomarkers. *Talanta* **2019**, *195*, 62–68. [CrossRef]
71. Boonkaew, S.; Jang, I.; Noviana, E.; Siangproh, W.; Chailapakul, O.; Henry, C. Electrochemical Paper-Based Analytical Device for Multiplexed, Point-of-Care Detection of Cardiovascular Disease Biomarkers. *Sens. Actuators B Chem.* **2021**, *330*, 129336. [CrossRef]
72. Dave, K.; Pachauri, N.; Dinda, A.; Solanki, P. RGO Modified Mediator Free Paper for Electrochemical Biosensing Platform. *Appl. Surf. Sci.* **2019**, *463*, 587–595. [CrossRef]
73. Wang, Y.; Sun, S.; Luo, J.; Xiong, Y.; Ming, T.; Liu, J.; Ma, Y.; Yan, S.; Yang, Y.; Yang, Z.; et al. Low Sample Volume Origami-Paper-Based Graphene-Modified Aptasensors for Label-Free Electrochemical Detection of Cancer Biomarker-EGFR. *Microsyst. Nanoeng.* **2020**, *6*, 32. [CrossRef]
74. Ming, T.; Cheng, Y.; Xing, Y.; Luo, J.; Mao, G.; Liu, J.; Sun, S.; Kong, F.; Jin, H.; Cai, X. Electrochemical Microfluidic Paper-Based Aptasensor Platform Based on a Biotin-Streptavidin System for Label-Free Detection of Biomarkers. *ACS Appl. Mater. Interfaces* **2021**, *13*, 46317–46324. [CrossRef]
75. Wei, X.; Guo, J.; Lian, H.; Sun, X.; Liu, B. Cobalt Metal-Organic Framework Modified Carbon Cloth/Paper Hybrid Electrochemical Button-Sensor for Nonenzymatic Glucose Diagnostics. *Sens. Actuators B Chem.* **2021**, *329*, 129205. [CrossRef]
76. Zhou, C.; Cui, K.; Liu, Y.; Hao, S.; Zhang, L.; Ge, S.; Yu, J. Ultrasensitive Microfluidic Paper-Based Electrochemical/Visual Analytical Device via Signal Amplification of Pd@Hollow Zn/Co Core-Shell ZIF67/ZIF8 Nanoparticles for Prostate-Specific Antigen Detection. *Anal. Chem.* **2021**, *93*, 5459–5467. [CrossRef] [PubMed]
77. Lu, Q.; Su, T.; Shang, Z.; Jin, D.; Shu, Y.; Xu, Q.; Hu, X. Flexible Paper-Based Ni-MOF Composite/AuNPs/CNTs Film Electrode for HIV DNA Detection. *Biosens. Bioelectron.* **2021**, *184*, 113229. [CrossRef]
78. Ma, C.; Cao, Y.; Gou, X.; Zhu, J.-J. Recent Progress in Electrochemiluminescence Sensing and Imaging. *Anal. Chem.* **2020**, *92*, 431–454. [CrossRef] [PubMed]
79. Xie, L.S.; Skorupskii, G.; Dincă, M. Electrically Conductive Metal–Organic Frameworks. *Chem. Rev.* **2020**, *120*, 8536–8580. [CrossRef]
80. Choleva, T.G.; Kappi, F.A.; Giokas, D.L.; Vlessidis, A.G. Paper-Based Assay of Antioxidant Activity Using Analyte-Mediated on-Paper Nucleation of Gold Nanoparticles as Colorimetric Probes. *Anal. Chim. Acta* **2015**, *860*, 61–69. [CrossRef]
81. Alba-Patiño, A.; Russell, S.M.; Rica, R. Origami-Enabled Signal Amplification for Paper-Based Colorimetric Biosensors. *Sens. Actuators B Chem.* **2018**, *273*, 951–954. [CrossRef]
82. Xie, L.; Zi, X.; Zeng, H.; Sun, J.; Xu, L.; Chen, S. Low-Cost Fabrication of a Paper-Based Microfluidic using a Folded Pattern Paper. *Anal. Chim. Acta* **2019**, *1053*, 131–138. [CrossRef]
83. Liang, P.; Yu, H.; Guntupalli, B.; Xiao, Y. Paper-Based Device for Rapid Visualization of NADH Based on Dissolution of Gold Nanoparticles. *ACS Appl. Mater. Interfaces* **2015**, *7*, 15023–15030. [CrossRef]
84. Liu, C.; Miao, Y.; Zhang, X.; Zhang, S.; Zhao, X. Colorimetric Determination of Cysteine by a Paper-Based Assay System using Aspartic Acid Modified Gold Nanoparticles. *Microchim. Acta* **2020**, *187*, 362. [CrossRef]
85. Díaz-Amaya, S.; Zhao, M.; Allebach, J.P.; Chiu, G.T.-C.; Stanciu, L.A. Ionic Strength Influences on Biofunctional Au-Decorated Microparticles for Enhanced Performance in Multiplexed Colorimetric Sensors. *ACS Appl. Mater. Interfaces* **2020**, *12*, 32397–32409. [CrossRef] [PubMed]
86. Tsai, T.-T.; Huang, C.-Y.; Chen, C.-A.; Shen, S.-W.; Wang, M.-C.; Cheng, C.-M.; Chen, C.-F. Diagnosis of Tuberculosis Using Colorimetric Gold Nanoparticles on a Paper-Based Analytical Device. *ACS Sens.* **2017**, *2*, 1345–1354. [CrossRef] [PubMed]
87. Huang, J.-Y.; Lin, H.-T.; Chen, T.-H.; Chen, C.-A.; Chang, H.-T.; Chen, C.-F. Signal Amplified Gold Nanoparticles for Cancer Diagnosis on Paper-Based Analytical Devices. *ACS Sens.* **2018**, *3*, 174–182. [CrossRef]

88. Sena-Torralba, A.; Alvarez-Diduk, R.; Parolo, C.; Torné-Morató, H.; Müller, A.; Merkoçi, A. Paper-Based Electrophoretic Bioassay: Biosensing in Whole Blood Operating via Smartphone. *Anal. Chem.* **2021**, *93*, 3112–3121. [[CrossRef](#)] [[PubMed](#)]
89. Devadhasan, J.P.; Gu, J.; Chen, P.; Smith, S.; Thomas, B.; Gates-Hollingsworth, M.; Hau, D.; Pandit, S.; AuCoin, D.; Zenhausem, F. Critical Comparison between Large and Mini Vertical Flow Immunoassay Platforms for *Yersinia Pestis* Detection. *Anal. Chem.* **2021**, *93*, 9337–9344. [[CrossRef](#)]
90. Lei, K.F.; Huang, C.-H.; Kuo, R.-L.; Chang, C.-K.; Chen, K.-F.; Tsao, K.-C.; Tsang, N.-M. Paper-Based Enzyme-Free Immunoassay for Rapid Detection and Subtyping of Influenza A H1N1 and H3N2 Viruses. *Anal. Chim. Acta* **2015**, *883*, 37–44. [[CrossRef](#)]
91. Xu, F.Q.; Zhu, Q.Y.; Zhang, H.; Wang, Z.X. Preparation of Colloidal Gold-Labeled Immunochromatographic Strips for Detection of Soluble Interleukin-2 Receptors in Real Samples. *Chinese J. Anal. Chem.* **2021**, *49*, 973–981.
92. Pang, R.Z.; Zhu, Q.Y.; Wei, J.; Wang, Y.Q.; Xu, F.Q.; Meng, X.Y.; Wang, Z.X. Development of a Gold-Nanorod-Based Lateral Flow Immunoassay for a Fast and Dual-Modal Detection of C-Reactive Protein in Clinical Plasma Samples. *RSC Adv.* **2021**, *11*, 28388–28394. [[CrossRef](#)]
93. Li, F.; Guo, L.; Hu, Y.; Li, Z.; Liu, J.; He, J.; Cui, H. Multiplexed Chemiluminescence Determination of Three Acute Myocardial Infarction Biomarkers Based on Microfluidic Paper-Based Immunodevice Dual Amplified by Multifunctionalized Gold Nanoparticles. *Talanta* **2020**, *207*, 120346. [[CrossRef](#)]
94. Ying, B.; Park, S.; Chen, L.; Dong, X.; Young, E.W.K.; Liu, X. NanoPADs and NanoFACEs: An Optically Transparent Nanopaper-Based Device for Biomedical Applications. *Lab Chip* **2020**, *20*, 3322–3333. [[CrossRef](#)]
95. Liu, Y.-C.; Hsu, C.-H.; Lu, B.-J.; Lin, P.-Y.; Ho, M.-L. Determination of Nitrite Ions in Environment Analysis with a Paper-Based Microfluidic Device. *Dalton Trans.* **2018**, *47*, 14799–14807. [[CrossRef](#)]
96. Monisha; Shrivasa, K.; Kant, T.; Patel, S.; Devi, R.; Dahariya, N.S.; Pervez, S.; Deb, M.K.; Rai, M.K.; Rai, J. Inkjet-Printed Paper-Based Colorimetric Sensor Coupled with Smartphone for Determination of Mercury ( $Hg^{2+}$ ). *J. Hazard. Mater.* **2021**, *414*, 125440. [[CrossRef](#)]
97. Ferreira, D.C.M.; Giordano, G.F.; Soares, C.; De Oliveira, J.; Mendes, R.; Piazzetta, M.; Gobbi, A.; Cardoso, M. Optical Paper-Based Sensor for Ascorbic Acid Quantification using Silver Nanoparticles. *Talanta* **2015**, *141*, 188–194. [[CrossRef](#)]
98. Mettakoonpitak, J.; Khongsoun, K.; Wongwan, N.; Kaewbutdee, S.; Siripinyanond, A.; Kuharuk, A.; Henry, C.S. Simple Biodegradable Plastic Screen-Printing for Microfluidic Paper-Based Analytical Devices. *Sens. Actuators B Chem.* **2021**, *331*, 129463. [[CrossRef](#)]
99. Firdaus, M.L.; Aprian, A.; Meileza, N.; Hitsmi, M.; Elvia, R.; Rahmidar, L.; Khaydarov, R. Smartphone Coupled with a Paper-Based Colorimetric Device for Sensitive and Portable Mercury Ion Sensing. *Chemosensors* **2019**, *7*, 25. [[CrossRef](#)]
100. Mavaei, M.; Chahardoli, A.; Fattahi, A.; Khoshroo, A. A Simple Method for Developing a Hand-Drawn Paper-Based Sensor for Mercury; Using Green Synthesized Silver Nanoparticles and Smartphone as a Hand-Held-Device for Colorimetric Assay. *Glob. Chall.* **2021**, *5*, 2000099. [[CrossRef](#)] [[PubMed](#)]
101. Shrivasa, K.; Patel, M.; Thakur, S.; Shankar, R. Food Safety Monitoring of the Pesticide Phenthoate using a Smartphone-Assisted Paperbased Sensor with Bimetallic Cu@Ag Core-Shell Nanoparticles. *Lab Chip* **2020**, *20*, 3996–4006. [[CrossRef](#)] [[PubMed](#)]
102. Fakhri, N.; Abarghoei, S.; Dadmehr, M.; Hosseini, M.; Sabahi, H.; Ganjali, M. Paper Based Colorimetric Detection of miRNA-21 using Ag/Pt Nanoclusters. *Spectrochim. Acta A* **2020**, *227*, 117529. [[CrossRef](#)] [[PubMed](#)]
103. Shi, L.; Liu, W.; Li, B.; Yang, C.J.; Jin, Y. Multichannel Paper Chip-Based Gas Pressure Bioassay for Simultaneous Detection of Multiple MicroRNAs. *ACS Appl. Mater. Interfaces* **2021**, *13*, 15008–15016. [[CrossRef](#)] [[PubMed](#)]
104. Zhang, W.; Niua, X.; Li, X.; He, Y.; Song, H.; Peng, Y.; Pan, J.; Qiu, F.; Zhao, H.; Lan, M. A Smartphone-Integrated Ready-to-Use Paper-Based Sensor with Mesoporous Carbon-Dispersed Pd Nanoparticles as a Highly Active Peroxidase Mimic for  $H_2O_2$  Detection. *Sens. Actuators B Chem.* **2018**, *265*, 412–420. [[CrossRef](#)]
105. Feng, L.-X.; Tang, C.; Han, X.-X.; Zhang, H.-C.; Guo, F.-N.; Yang, T.; Wang, J.-H. Simultaneous and Sensitive Detection of Multiple Small Biological Molecules by Microfluidic Paper-Based Analytical Device Integrated with Zinc Oxide Nanorods. *Talanta* **2021**, *232*, 122499. [[CrossRef](#)]
106. Jamil, S.; Nasir, M.; Ali, Y.; Nadeem, S.; Rashid, S.; Javed, M.Y.; Hayat, A.  $Cr_2O_3$ – $TiO_2$ -Modified Filter Paper-Based Portable Nanosensors for Optical and Colorimetric Detection of Hydrogen Peroxide. *ACS Omega* **2021**, *6*, 23368–23377. [[CrossRef](#)]
107. Sawetwong, P.; Chairam, S.; Jarujamrus, P.; Amatongchai, M. Enhanced Selectivity and Sensitivity for Colorimetric Determination of Glyphosate using Mn–ZnS Quantum Dot Embedded Molecularly Imprinted Polymers Combined with a 3D-Microfluidic Paper-Based Analytical Device. *Talanta* **2021**, *225*, 122077. [[CrossRef](#)]
108. Kitchawengkul, N.; Prakobkij, A.; Anutrasakda, W.; Yodsins, N.; Jungsuttiwong, S.; Chunta, S.; Amatongchai, M.; Jarujamrus, P. Mimicking Peroxidase-Like Activity of Nitrogen-Doped Carbon Dots (N-CDs) Coupled with a Laminated Three-Dimensional Microfluidic Paper-Based Analytical Device (Laminated 3D- $\mu$ PAD) for Smart Sensing of Total Cholesterol from Whole Blood. *Anal. Chem.* **2021**, *93*, 6989–6999. [[CrossRef](#)]
109. Liu, C.; Luo, Y.; Wen, H.; Qi, Y.; Shi, G.; Deng, J.; Zhou, T. Red-to-Blue Paper-Based Colorimetric Sensor Integrated with Smartphone for Point-of-Use Analysis of Cerebral AChE upon  $Cd^{2+}$  Exposure. *Nanoscale* **2021**, *13*, 1283–1290. [[CrossRef](#)]
110. Huy, B.; Nghia, N.; Lee, Y.-I. Highly Sensitive Colorimetric Paper-Based Analytical Device for the Determination of Tetracycline using Green Fluorescent Carbon Nitride Nanoparticles. *Microchem. J.* **2020**, *158*, 105151. [[CrossRef](#)]
111. Pimentel, E.S.; Brito-Pereira, R.; Marques-Almeida, T.; Ribeiro, C.; Vaz, F.; Lanceros-Mendez, S.; Cardoso, V.F. Tailoring Electrospun Poly(L-lactic acid) Nanofibers as Substrates for Microfluidic Applications. *ACS Appl. Mater. Interfaces* **2020**, *12*, 60–69. [[CrossRef](#)]

112. Lawati, H.; Hassanzadeh, J. Dual-Function 2D Cobalt Metal-Organic Framework Embedded on Paper as a Point-of-Care Diagnostic Device: Application for the Quantification of Glucose. *Anal. Chim. Acta* **2020**, *1139*, 15–26. [[CrossRef](#)]
113. Marín-Barroso, E.; Moreira, C.M.; Messina, G.A.; Bertolino, F.A.; Alderete, M.; Soler-Illia, G.J.A.A.; Raba, J.; Pereira, S.V. Paper Based Analytical Device Modified with Nanoporous Material for the Fluorescent Sensing of Gliadin Content in Different Food Samples. *Microchem. J.* **2018**, *142*, 78–84. [[CrossRef](#)]
114. Tang, X.; Zhang, Q.; Zhang, Z.; Ding, X.; Jiang, J.; Zhang, W.; Li, P. Rapid, On-Site and Quantitative Paper-Based Immunoassay Platform for Concurrent Determination of Pesticide Residues and Mycotoxins. *Anal. Chim. Acta* **2019**, *1078*, 142–150. [[CrossRef](#)] [[PubMed](#)]
115. Wu, X.-J.; Kong, F.; Zhao, C.-Q.; Ding, S.-N. Ratiometric Fluorescent Nanosensors for Ultra-Sensitive Detection of Mercury Ions Based on AuNCs/MOFs. *Analyst* **2019**, *144*, 2523–2530. [[CrossRef](#)]
116. Ungor, D.; Horváth, K.; Dékány, I.; Csapó, E. Red-Emitting Gold Nanoclusters for Rapid Fluorescence Sensing of Tryptophan Metabolites. *Sens. Actuators B Chem.* **2019**, *288*, 728–733. [[CrossRef](#)]
117. Lert-itthiporn, A.; Srikritsawong, P.; Choengchan, N. Foldable Paper-Based Analytical Device for Membraneless Gas-Separation and Determination of Iodate Based on Fluorescence Quenching of Gold Nanoclusters. *Talanta* **2021**, *221*, 121574. [[CrossRef](#)] [[PubMed](#)]
118. Pena-Pereira, F.; Capón, N.; Calle, I.; Lavilla, I.; Bendicho, C. Fluorescent Poly(vinylpyrrolidone)-Supported Copper Nanoclusters in Miniaturized Analytical Systems for Iodine Sensing. *Sens. Actuators B Chem.* **2019**, *299*, 126979. [[CrossRef](#)]
119. Yin, X.; Liang, L.; Zhao, P.; Lan, F.; Zhang, L.; Ge, S.; Yu, J. Double Signal Amplification Based on Palladium Nanoclusters and Nucleic Acid Cycles on a IPAD for Dual-Model Detection of MicroRNAs. *J. Mater. Chem. B* **2018**, *6*, 5795–5801. [[CrossRef](#)] [[PubMed](#)]
120. Wang, M.; Song, Z.; Jiang, Y.; Zhang, X.; Wang, L.; Zhao, H.; Cui, Y.; Gu, F.; Wang, Y.; Zheng, G. A Three-Dimensional Pinwheel-Shaped Paper-Based Microfluidic Analytical Device for Fluorescence Detection of Multiple Heavy Metals in Coastal Waters by Rational Device Design. *Anal. Bioanal. Chem.* **2021**, *413*, 3299–3313. [[CrossRef](#)]
121. Liu, Q.; Lin, Y.; Xiong, J.; Wu, L.; Hou, X.; Xu, K.; Zheng, C. Disposable Paper-Based Analytical Device for Visual Speciation Analysis of Ag(I) and Silver Nanoparticles (AgNPs). *Anal. Chem.* **2019**, *91*, 3359–3366. [[CrossRef](#)] [[PubMed](#)]
122. Zhang, Z.; Ma, X.; Li, B.; Zhao, J.; Qi, J.; Hao, G.; Rong, J.; Yang, X. Fluorescence Detection of 2,4-Dichlorophenoxyacetic Acid by Ratiometric Fluorescence Imaging on Paper-Based Microfluidic Chips. *Analyst* **2020**, *145*, 963–974. [[CrossRef](#)]
123. Thepmanee, O.; Prapainop, K.; Noppha, O.; Rattanawimanwong, N.; Siangproh, W.; Chailapakul, O.; Songsrirote, K. A Simple Paper-Based Approach for Arsenic Determination in Water using Hydride Generation Coupled with Mercaptosuccinic-Acid Capped CdTe Quantum Dots. *Anal. Methods* **2020**, *12*, 2718–2726. [[CrossRef](#)]
124. Kuang, Y.; Wang, X.; Tian, X.; Yang, C.; Li, Y.; Nie, Y. Silica-Embedded CdTe Quantum Dots Functionalized with Rhodamine Derivative for Instant Visual Detection of Ferric Ions in Aqueous Media. *J. Photoch. Photobiol. A* **2019**, *372*, 140–146. [[CrossRef](#)]
125. Ou, Q.; Tawfik, S.M.; Zhang, X.; Lee, Y.-I. Novel “Turn On–Off” Paper Sensor Based on Nonionic Conjugated Polythiophene-Coated CdTe QDs for Efficient Visual Detection of Cholinesterase Activity. *Analyst* **2020**, *145*, 4305–4313. [[CrossRef](#)] [[PubMed](#)]
126. Guo, X.; Chen, Y.; Zhang, L.; Liu, W. An Inkjet Printing Paper-Based Immunodevice for Fluorescence Determination of Immunoglobulin G. *Anal. Methods* **2019**, *11*, 3452–3459. [[CrossRef](#)]
127. Huang, L.; Wang, J.; Wang, Q.; Tang, D.; Lin, Y. Distance-Dependent Visual Fluorescence Immunoassay on CdTe Quantum Dot-Impregnated Paper through Silver Ion-Exchange Reaction. *Microchim. Acta* **2020**, *187*, 563. [[CrossRef](#)]
128. Moreira, C.M.; Marín-Barroso, E.; Pereira, S.V.; Raba, J.; Messina, G.A.; Bertolino, F.A. A Nanostructured Paper-Based Device for Phenylalanine Neonatal Screening by LED-Induced Fluorescence. *Anal. Methods* **2020**, *12*, 1624–1630. [[CrossRef](#)]
129. Lin, Y.-H.; Yeh, Y.-C. Rapid Synthesis of Microwave-Assisted Zinc Oxide Nanorods on a Paper-Based Analytical Device for Fluorometric Detection of L-Dopa. *Colloids Surf. B* **2021**, *207*, 111995. [[CrossRef](#)]
130. Zhao, M.; Li, H.; Liu, W.; Chu, W.; Chen, Y. Paper-Based Laser Induced Fluorescence Immunodevice Combining with CdTe Embedded Silica Nanoparticles Signal Enhancement Strategy. *Sens. Actuators B Chem.* **2017**, *242*, 87–94. [[CrossRef](#)]
131. Qiu, Z.; Shu, J.; Tang, D. Bioresponsive Release System for Visual Fluorescence Detection of Carcinoembryonic Antigen from Mesoporous Silica Nanocontainers Mediated Optical Color on Quantum Dot-Enzyme-Impregnated Paper. *Anal. Chem.* **2017**, *89*, 5152–5160. [[CrossRef](#)]
132. Zhou, J.; Li, B.; Qi, A.; Shi, Y.; Qi, J.; Xu, H.; Chen, L. ZnSe Quantum Dot Based Ion Imprinting Technology for Fluorescence Detecting Cadmium and Lead Ions on a Three-Dimensional Rotary Paper-Based Microfluidic Chip. *Sens. Actuators B Chem.* **2020**, *305*, 127462. [[CrossRef](#)]
133. Noor, M.O.; Hrovat, D.; Moazami-Goudarzi, M.; Espie, G.S.; Krull, U.J. Ratiometric Fluorescence Transduction by Hybridization after Isothermal Amplification for Determination of Zeptomole Quantities of Oligonucleotide Biomarkers with a Paper-Based Platform and Camera-Based Detection. *Anal. Chim. Acta* **2015**, *885*, 156–165. [[CrossRef](#)]
134. Xia, Z.; Li, D.; Deng, W. Identification and Detection of Volatile Aldehydes as Lung Cancer Biomarkers by Vapor Generation Combined with Paper-Based Thin Film Microextraction. *Anal. Chem.* **2021**, *93*, 4924–4931. [[CrossRef](#)] [[PubMed](#)]
135. Liang, L.; Lan, F.; Li, L.; Su, M.; Ge, S.; Yu, J.; Liu, H.; Yan, M. Fluorescence “Turn-On” Determination of H<sub>2</sub>O<sub>2</sub> using Multilayer Porous SiO<sub>2</sub>/NGQDs and PdAu Mimetics Enzymatic/Oxidative Cleavage of Single-Stranded DNA. *Biosens. Bioelectron.* **2016**, *82*, 204–211. [[CrossRef](#)]

136. Wang, X.; Hou, J.; Lan, S.; Shen, C.; Huo, D.; Ji, Z.; Ma, Y.; Luo, H.; Zhang, S.; He, Q.; et al. MoS<sub>2</sub> QDs-Based Sensor for Measurement of Fluazinam with Triple Signal Output. *Anal. Chim. Acta* **2020**, *1108*, 152–159. [[CrossRef](#)] [[PubMed](#)]
137. Apilux, W.; Siangproh, N.; Insin, O.C.; Prachayasittikul, V. Paper-Based Thioglycolic Acid (TGA)-Capped CdTe QD Device for Rapid Screening of Organophosphorus and Carbamate Insecticides. *Anal. Methods* **2017**, *9*, 519–527. [[CrossRef](#)]
138. El-Shaheny, R.; Yoshida, S.; Fuchigami, T. Graphene Quantum Dots as a Nanoprobe for Analysis of O- and P-nitrophenols in Environmental Water Adopting Conventional Fluorometry and Smartphone Image Processing-Assisted Paper-Based Analytical Device. *Microchem. J.* **2020**, *158*, 105241. [[CrossRef](#)]
139. Shah, K.G.; Singh, V.; Kauffman, P.C.; Abe, K.; Yager, P. Mobile Phone Ratiometric Imaging Enables Highly Sensitive Fluorescence Lateral Flow Immunoassays without External Optical Filters. *Anal. Chem.* **2018**, *90*, 6967–6974. [[CrossRef](#)]
140. Liang, L.; Su, M.; Li, L.; Lan, F.; Yang, G.; Ge, S.; Yu, J.; Song, X. Aptamer-Based Fluorescent and Visual Biosensor for Multiplexed Monitoring of Cancer Cells in Microfluidic Paper-Based Analytical Devices. *Sens. Actuators B Chem.* **2016**, *229*, 347–354. [[CrossRef](#)]
141. Ye, J.; Geng, Y.; Cao, F.; Sun, D.; Xu, S.; Chang, J.; Xu, W.; Chen, Q. A Smartphone-Assisted Paper-Based Analytical Device for Fluorescence Assay of Hg<sup>2+</sup>. *Chem. Res. Chin. Univ.* **2019**, *35*, 972–977. [[CrossRef](#)]
142. Ninwong, B.; Sangkaew, P.; Hapa, P.; Ratnarathorn, N.; Menger, R.F.; Henry, C.S.; Dungchai, W. Sensitive Distance-Based Paper-Based Quantification of Mercury Ions Using Carbon Nanodots and Heating-Based Preconcentration. *RSC Adv.* **2020**, *10*, 9884–9893. [[CrossRef](#)]
143. Li, W.; Zhang, X.; Miao, C.; Li, R.; Ji, Y. Fluorescent Paper-Based Sensor Based on Carbon Dots for Detection of Folic Acid. *Anal. Bioanal. Chem.* **2020**, *412*, 2805–2813. [[CrossRef](#)]
144. Wang, H.; Yang, L.; Chu, S.; Liu, B.; Zhang, Q.; Zou, L.; Yu, S.; Jiang, C. Semiquantitative Visual Detection of Lead Ions with a Smartphone via a Colorimetric Paper-Based Analytical Device. *Anal. Chem.* **2019**, *91*, 9292–9299. [[CrossRef](#)]
145. Hu, J.; Yang, X.; Peng, Q.; Wang, F.; Zhu, Y.; Hu, X.; Zheng, B.; Du, J.; Xiao, D. A Highly Sensitive Visual Sensor for Tetracycline in Food Samples by a Double-Signal Response Fluorescent Nanohybrid. *Food Control* **2020**, *108*, 106832. [[CrossRef](#)]
146. Yehia, A.M.; Farag, M.A.; Tantawy, M.A. A Novel Trimodal System on a Paper-Based Microfluidic Device for Onsite Detection of the Date Rape Drug “Ketamine”. *Anal. Chim. Acta* **2020**, *1104*, 95–104. [[CrossRef](#)]
147. Ortiz-Gomez, I.; Ortega-Muñoz, M.; Marín-Sánchez, A.; de Orbe-Payá, I.; Hernandez-Mateo, F.; Capitan-Vallvey, L.; Santoyo-Gonzalez, F.; Salinas-Castillo, A. A Vinyl Sulfone Clicked Carbon Dot-Engineered Microfluidic Paper-Based Analytical Device for Fluorometric Determination of Biothiols. *Microchim. Acta* **2020**, *187*, 421. [[CrossRef](#)] [[PubMed](#)]
148. Zhang, X.; Chen, S.; Zhuo, S.; Ji, Y.; Li, R. A Carbon Dots Functionalized Paper Coupled with AgNPs Composites Platform: Application as a Sensor for Hydrogen Peroxide Detection Based on Surface Plasmon-Enhanced Energy Transfer. *New J. Chem.* **2021**, *45*, 6025–6032. [[CrossRef](#)]
149. Tian, X.; Wang, J.; Li, Y.; Yang, C.; Lu, L.; Nie, Y. Sensitive Determination of Hardness and Fluoride in Ground Water by a Hybrid Nanosensor Based on Aggregation Induced FRET On and Off Mechanism. *Sens. Actuators B Chem.* **2018**, *262*, 522–530. [[CrossRef](#)]
150. Ortiz-Gomez, I.; Toral-Lopez, V.; Romero, F.J.; De Orbe-Paya, I.; García, A.; Rodríguez, N.; Capitan-Vallvey, L.; Morales, D.; Salinas-Castillo, A. In Situ Synthesis of Fluorescent Silicon Nanodots for Determination of Total Carbohydrates in a Paper Microfluidic Device Combined with Laser Prepared Graphene Heater. *Sens. Actuators B Chem.* **2021**, *332*, 129506. [[CrossRef](#)]
151. Liang, L.; Lan, F.; Yin, X.; Ge, S.; Yu, J.; Yan, M. Metal-Enhanced Fluorescence/Visual Bimodal Platform for Multiplexed Ultrasensitive Detection of MicroRNA with Reusable Paper Analytical Devices. *Biosens. Bioelectron.* **2017**, *95*, 181–188. [[CrossRef](#)]
152. El-Shaheny, R.; Al-Khateeb, L.A.; El-Maghrabey, M. Dual-Excitation In-Lab-Made Device Based on a Handy UV Lamp and GQDs-Modified PADs for Simultaneous Determination of Acetaminophen and Its Endocrine Disrupting Impurity 4-Nitrophenol. *Sens. Actuators B Chem.* **2021**, *348*, 130657. [[CrossRef](#)]
153. Wang, F.M.; Li, W.; Wang, J.S.; Ren, J.S.; Qu, X.G. Detection of Telomerase on Upconversion Nanoparticle Modified Cellulose Paper. *Chem. Commun.* **2015**, *51*, 11630–11633. [[CrossRef](#)] [[PubMed](#)]
154. Huang, Z.; Liu, Y.H.; Chen, Y.; Xiong, Q.R.; Wang, Y.H.; Duan, H.W.; Lai, W.H. Improving the Performance of Upconversion Nanoprobe-Based Lateral Flow Immunoassays by Supramolecular Self-Assembly Core/Shell Strategies. *Sens. Actuators B Chem.* **2020**, *318*, 128233. [[CrossRef](#)]
155. He, M.; Shang, N.; Zhu, Q.; Xu, J. Paper-Based Upconversion Fluorescence Aptasensor for the Quantitative Detection of Immunoglobulin E in Human Serum. *Anal. Chim. Acta* **2021**, *1143*, 93–100. [[CrossRef](#)]
156. Na, M.; Zhang, S.; Liu, J.; Ma, S.; Han, Y.; Wang, Y.; He, Y.; Chen, H.; Chen, X. Determination of Pathogenic Bacteria—Bacillus Anthrax Spores in Environmental Samples by Ratiometric Fluorescence and Test Paper Based on Dual-Emission Fluorescent Silicon Nanoparticles. *J. Hazard. Mater.* **2020**, *386*, 121956. [[CrossRef](#)] [[PubMed](#)]
157. Lv, S.; Tang, Y.; Zhang, K.; Tang, D. Wet NH<sub>3</sub>-Triggered NH<sub>2</sub>-MIL-125(Ti) Structural Switch for Visible Fluorescence Immunoassay Impregnated on Paper. *Anal. Chem.* **2018**, *90*, 14121–14125. [[CrossRef](#)]
158. Yu, L.; Zheng, Q.; Wang, H.; Liu, C.; Huang, X.; Xiao, Y. Double-Color Lanthanide Metal–Organic Framework Based Logic Device and Visual Ratiometric Fluorescence Water Microsensor for Solid Pharmaceuticals. *Anal. Chem.* **2020**, *92*, 1402–1408. [[CrossRef](#)] [[PubMed](#)]
159. Yu, L.; He, C.; Zheng, Q.; Feng, L.; Xiong, L.; Xiao, Y. Dual Eu-MOFs Based Logic Device and Ratiometric Fluorescence Paper Microchip for Visual H<sub>2</sub>O<sub>2</sub> Assay. *J. Mater. Chem. C* **2020**, *8*, 3562–3570. [[CrossRef](#)]

160. Zhang, D.; Du, P.; Chen, J.; Guo, H.; Lu, X. Pyrazolate-Based Porphyrinic Metal-Organic Frameworks as Catechol Oxidase Mimic Enzyme for Fluorescent and Colorimetric Dual-Mode Detection of Dopamine with High Sensitivity and Specificity. *Sens. Actuators B Chem.* **2021**, *341*, 130000. [[CrossRef](#)]
161. Yue, X.; Li, Y.; Xu, S.; Li, J.; Li, M.; Jiang, L.; Jie, M.; Bai, Y. A Portable Smartphone-Assisted Ratiometric Fluorescence Sensor for Intelligent and Visual Detection of Malachite Green. *Food Chem.* **2022**, *371*, 131164. [[CrossRef](#)]
162. Abbas, A.; Brimer, A.; Slocik, J.M.; Tian, L.; Naik, R.R.; Singamaneni, S. Multifunctional Analytical Platform on a Paper Strip: Separation, Preconcentration, and Subattomolar Detection. *Anal. Chem.* **2013**, *85*, 3977–3983. [[CrossRef](#)] [[PubMed](#)]
163. Torul, H.; Çiftçi, H.; Çetin, D.; Suludere, Z.; Boyacı, I.; Tamer, U. Paper Membrane-Based SERS Platform for the Determination of Glucose in Blood Samples. *Anal. Bioanal. Chem.* **2015**, *407*, 8243–8251. [[CrossRef](#)] [[PubMed](#)]
164. Kong, X.; Chong, X.; Squire, K.; Wang, A.X. Microfluidic Diatomite Analytical Devices for Illicit Drug Sensing with ppb-Level Sensitivity. *Sens. Actuators B Chem.* **2018**, *259*, 587–595. [[CrossRef](#)]
165. Choi, S.; Moon, S.; Lee, S.; Kim, W.; Kim, S.; Kim, S.; Shin, J.-H.; Park, Y.-G.; Jin, K.-H.; Kim, T. A Recyclable CNC-Milled Microfluidic Platform for Colorimetric Assays and Label-Free Aged-Related Macular Degeneration Detection. *Sens. Actuators B Chem.* **2019**, *290*, 484–492. [[CrossRef](#)]
166. Zheng, T.; Gao, Z.; Luo, Y.; Liu, X.; Zhao, W.; Lin, B. Manual-Slide-Engaged Paper Chip for Parallel SERS-Immunoassay Measurement of Clenbuterol from Swine Hair. *Electrophoresis* **2016**, *37*, 418–424. [[CrossRef](#)]
167. Huang, Z.; Siddhanta, S.; Zhang, C.; Kickler, T.; Zheng, G.; Barman, I. Painting and Heating: A Nonconventional, Scalable Route to Sensitive Biomolecular Analysis with Plasmon-Enhanced Spectroscopy. *J. Raman Spectrosc.* **2017**, *48*, 1365–1374. [[CrossRef](#)]
168. Li, H.; Geng, W.; Hassan, M.; Zuo, M.; Wei, W.; Wu, X.; Ouyang, Q.; Chen, Q. Rapid Detection of Chloramphenicol in Food Using SERS Flexible Sensor Coupled Artificial Intelligent Tools. *Food Control* **2021**, *128*, 108186. [[CrossRef](#)]
169. Tegegne, W.; Su, W.; Beyene, A.; Huang, W.; Tsai, M.; Hwang, B. Flexible Hydrophobic Filter Paper-Based SERS Substrate Using Silver Nanocubes for Sensitive and Rapid Detection of Adenine. *Microchem. J.* **2021**, *168*, 106349. [[CrossRef](#)]
170. Duan, H.; Deng, W.; Gan, Z.; Li, D.; Li, D. SERS-Based Chip for Discrimination of Formaldehyde and Acetaldehyde in Aqueous Solution using Silver Reduction. *Microchim. Acta* **2019**, *186*, 175. [[CrossRef](#)]
171. Qi, L.; Xiao, M.; Wang, X.; Wang, C.; Wang, L.; Song, S.; Qu, X.; Li, L.; Shi, J.; Pei, H. DNA-Encoded Raman-Active Anisotropic Nanoparticles for microRNA Detection. *Anal. Chem.* **2017**, *89*, 9850–9856. [[CrossRef](#)]
172. Li, D.; Duan, H.; Ma, Y.; Deng, W. Headspace-Sampling Paper-Based Analytical Device for Colorimetric/Surface-Enhanced Raman Scattering Dual Sensing of Sulfur Dioxide in Wine. *Anal. Chem.* **2018**, *90*, 5719–5727. [[CrossRef](#)] [[PubMed](#)]
173. Saha, A.; Jana, N.R. Paper-Based Microfluidic Approach for Surface-Enhanced Raman Spectroscopy and Highly Reproducible Detection of Proteins beyond Picomolar Concentration. *ACS Appl. Mater. Interfaces* **2015**, *7*, 996–1003. [[CrossRef](#)] [[PubMed](#)]
174. Wu, L.; Zhang, W.; Liu, C.; Foda, M.; Zhu, Y. Strawberry-Like SiO<sub>2</sub>/Ag Nanocomposites Immersed Filter Paper as SERS Substrate for Acrylamide Detection. *Food Chem.* **2020**, *328*, 127106. [[CrossRef](#)]
175. Chen, M.; Yang, H.; Rong, L.; Chen, X. A Gas-Diffusion Microfluidic Paper-Based Analytical Device (μPAD) Coupled with Portable Surface-Enhanced Raman Scattering (SERS): Facile Determination of Sulphite in Wines. *Analyst* **2016**, *141*, 5511–5519. [[CrossRef](#)] [[PubMed](#)]
176. Lan, L.; Hou, X.; Gao, Y.; Fan, X.; Qiu, T. Inkjet-Printed Paper-Based Semiconducting Substrates for Surface-Enhanced Raman Spectroscopy. *Nanotechnology* **2020**, *31*, 055502. [[CrossRef](#)]